The within-subject stability of cortical thickness, surface area, and brain volumes across one year

Meng-Yun Wang[1,2,3,4], Max Korbmacher[4,5], Rune Eikeland[1,4], Stener Nerland[6,7], Didac Vidal-Pineiro[8], Karsten Specht[1,4,9]

1. Department of Biological and Medical Psychology, University of Bergen, Bergen, Norway

2. Language and Genetics Department, Max Planck Institute for Psycholinguistics, Nijmegen, Netherlands

3. Donders Institute for Brain, Cognition and Behavior, Radboud University, Nijmegen, Netherlands

4. Mohn Medical Imaging and Visualization Centre (MMIV), Haukeland University Hospital, Bergen, Norway

5. Department of Health and Functioning, Western Norway University of Applied Sciences, Bergen, Norway

6. Department of Psychiatric Research, Diakonhjemmet Hospital, Oslo, Norway

7. Norwegian Center for Mental Disorders Research (NORMENT), Institute of Clinical Medicine, University of Oslo, Oslo, Norway

8. Center for Lifespan Changes in Brain and Cognition, Department of Psychology, University of Oslo, Oslo, Norway

9. Department of Education, UiT The Arctic University of Norway, Tromsø, Norway

*Correspondence: Karsten Specht, karsten.specht@uib.no or Meng-Yun Wang mengyun.wang@uib.no

Abstract:

T1-weighted (T1w) imaging is widely used to examine brain structure based on image-derived phenotypes (IDPs) such as cortical thickness, surface area, and brain volumes. The reliability of these IDPs has been extensively explored, mainly focusing on the inter-subject variations, whereas the stability of the within-subject variations has often been overlooked. Additionally, how environmental factors such as time of day and daylight hours impact the structural brain is poorly understood. Therefore, we aimed to assess the stability of T1w-derived phenotypes and explore the effects of time of day and daylight hours.

Three subjects in their late 20s, early 30s, and early 40s were scanned repeatedly on the same scanner over one year, from which a densely sampled dataset was acquired with 38, 40, and 25 sessions for subjects 1, 2, and 3, respectively. The temporal stability was evaluated using within-subject percentage change and coefficients of variance (CV). The effects of time of day and daylight hours were assessed by fitting general linear models, aggregating the effect size with meta-analysis, and equivalent analysis.

The majority of IDPs demonstrated percentage changes within 5% and CVs within 2% for the majority of brain regions, indicating fairly high stability. Interestingly, we found that the brain region size is negatively correlated with the CVs. Specifically, several small brain regions, including the temporal pole, frontal pole, pericalcarine, entorhinal cortex, and accumbens area, showed low stability. In addition, cortical thickness change was strongly and positively correlated with that of volume change while being negatively correlated with change in surface area, illustrating their distinct roles in brain anatomy. Moreover, the time of day could be ignored when evaluating the total surface area and total cortical brain volume but not average cortical thickness since we cannot rule out there is no actual time-of-day effect on it. Furthermore, daylight hours could be left out when evaluating IDPs since there is no appreciable effect of daylight hours on IDPs. Lastly, apparent head motion causes cortical thickness and volume to be underestimated and surface area to be overestimated.

Keywords: cortical thickness; surface area; volume; T1w; time-of-day; daylight hours; stability; head movement; reliability

1 Introduction

Magnetic resonance imaging (MRI) has become widely utilized to study brain structure, due to its ability to capture in vivo human brain images (Lerch et al., 2017). Commonly used T1-weighted (T1w) image-derived phenotypes (IDPs), including cortical thickness, surface area, and cortical as well as subcortical brain volumes, can be estimated with FreeSurfer, which is the most commonly used package for surface-based analysis (Dale, Fischl, & Sereno, 1999; Fischl, Sereno, & Dale, 1999). These IDPs have been ubiquitously used to investigate longitudinal brain changes (Bethlehem et al., 2022; Lemaitre et al., 2012; Sowell et al., 2003; Sowell et al., 2004; Vijayakumar et al., 2016), associations with other phenotypes (Chen et al., 2012; L. T. Elliott et al., 2018; Genon, Eickhoff, & Kharabian, 2022; Grasby et al., 2020; Holz et al., 2023; Wu, Li, Eickhoff, Scheinost, & Genon, 2023), and brain abnormalities in a variety of clinical conditions (Thompson et al., 2020).

However, before its grand application, the reliability and stability of the measurements should be articulated (Brandmaier et al., 2018). Reliability represents the contribution of the between-subject variance in terms of the total variance (sum of between- and within-subject variances) (Brandmaier et al., 2018; Zuo, Xu, & Milham, 2019) whereas stability refers to the precision of the within-subject estimations (Brandmaier et al., 2018). The reliability of the MRI measurements, which can be quantified with the intra-class correlation coefficient (ICC), has been extensively explored (Brandmaier et al., 2018; M. L. Elliott et al., 2020; Noble, Scheinost, & Constable, 2021; Noble et al., 2017; Parsons, Brandmaier, Lindenberger, & Kievit, 2024; Vidal-Piñeiro et al., 2024; Zuo et al., 2019). However, the stability of the MRI measurements has been largely ignored because of the scarcity of datasets with sufficient data points for each subject, which often leads to the presumption of taking the within-subject variance as a random error or noise (Brandmaier et al., 2018; Zuo et al., 2019).

Since the insufficiency of IDPs stability studies, it is still largely unknown which factor could sway the IDPs stability. Previous studies suggest that, among all the factors, different FreeSurfer versions (Gronenschild et al., 2012), operating systems (Gronenschild et al., 2012), scanners (Han et al., 2006; Iscan et al., 2015), processing streams (Reuter, Schmansky, Rosas, & Fischl, 2012; Vidal-Piñeiro et al., 2024), time of day (Karch et al., 2019; Nakamura et al., 2015; Trefler et al., 2016), daylight hours (Di, Woelfer, Kühn, Zhang, & Biswal, 2022), and head movement (Alexander-Bloch et al., 2016; Reuter et al., 2015) could affect the reliability or stability of the IDPs. The factor of the operating system and scanner can be controlled by a within-subject design, and the FreeSurfer version can be controlled by using the same version to process all the datasets. Thereafter, the remaining factors compassing processing stream, time of day, and daylight hours will be primarily investigated in this study.

There are two processing streams in FreeSurfer to calculate IDPs, namely the cross-sectional and longitudinal processing streams. The cross-sectional stream processes each scan independently while the longitudinal stream creates an unbiased within-subject template space and estimates IDPs based on all the available data for each participant (Reuter et al., 2012; Vidal-Piñeiro et al., 2024). However, the impact of the two streams on the within-subject stability level has not been fully uncovered. The CVs of those two streams, therefore, will be directly compared in this study.

Although time-of-day effects have been documented in functional brain organization studies (Orban, Kong, Li, Chee, & Yeo, 2020), the influence on brain structure is still elusive. Some studies have reported associations between time of day and cortical measures (Karch et al., 2019; Nakamura et al., 2015; Trefler et al., 2016). Specifically, the cortical thickness and brain volume are larger in the morning compared to the afternoon (Karch et al., 2019; Nakamura et al., 2015; Trefler et al., 2016). However, two of the studies (Nakamura et al.,

2015; Trefler et al., 2016) employed a cross-sectional design where between-subject variation could interfere with the reported time-of-day effect. For example, in one study, each subject only had two data points in their primary dataset for morning and afternoon sessions (Trefler et al., 2016), and the other study just pooled the data from other datasets and separated them based on the collection time (Nakamura et al., 2015). Although one is within-subject design (Karch et al., 2019), they did not use the longitudinal stream as recommended (Reuter, Schmansky, Rosas, & Fischl, 2012), which could hinder the robustness and reliability of the results. More critically, the data distributions of the morning and afternoon sessions within subjects are not illustrated. Therefore, in this study, within-subject design together with the longitudinal processing stream will be adopted meanwhile the data distribution will be provided.

Besides the time-of-day effect, the season of the year has been suggested to affect functional brain organization (M. Y. Wang, Korbmacher, Eikeland, & Specht, 2023b; Zhang, Shokri-Kojori, & Volkow, 2023). Specifically, daylight hours comes out as a potential contributor (Di et al., 2022) to the functional brain organization (M. Y. Wang et al., 2023b). For example, the salience network, one of the resting-state brain networks, is enlarged when daylight hours is short compared to when it is long (M. Y. Wang et al., 2023b). To the best of our knowledge, there is still no study investigating the daylight-hour effect on brain structure. Located right beneath the Arctic Circle, the daylight hours in Norway varies substantially throughout the year. Specifically, the daylight hours in the city of Bergen can be as short as around 2 hours of daylight and as long as around 16 hours of daylight, which makes it suitable for exploring the daylight-hour effect.

Low brain image quality can introduce bias which can lead to inaccurate and even erroneous results (Alexander-Bloch et al., 2016; Ducharme et al., 2016; Reuter et al., 2015). Brain images with obvious artifacts, such as field of view lacking parts of the brain, ringing artifacts, and image distortions are routinely discarded after visual inspection and are not used in further analysis. However, images that have passed the visual inspection can still influence the downstream processing. For example, the head movement can reduce gray matter volume and cortical thickness estimations (Alexander-Bloch et al., 2016; Reuter et al., 2015) and even micro-movement can influence the longitudinal brain change evaluations (Alexander-Bloch et al., 2016). However, a systematic overview of how within-subject head movement affects the estimation of IDPs is still lacking.

Therefore, the main aims of this study were twofold. First, to characterize the stability of IDPs, including cortical thickness, surface area, and brain volumes. Second, to investigate the influence of potential confounding variables on the stability of IDPs, specifically the effects of time of day, daylight hours, and head movement.

2 Methods

2.1 Participants

The ethics approval was granted by the Regional Committees for Medical and Health Research Ethics (REK-vest). Informed consent was obtained from all participants for being included in the study. Here, we collected a densely sampled brain imaging dataset derived from the BBSC (Bergen Breakfast Scanning Club) project (M. Y. Wang, Korbmacher, Eikeland, & Specht, 2022, 2023a). In this project, three subjects (**Table 1**) were repeatedly scanned in the same scanner located at the same place spanning over one year, which makes it suitable to evaluate IDPs stability (M. Y. Wang, Korbmacher, Eikeland, Craven, & Specht, 2024; M. Y. Wang et al., 2022). The BBSC project aims to illustrate the individual precision brain networks and to examine the stability of both functional and structural MRI

measurements over one year (M. Y. Wang et al., 2022). For this purpose, the participants were scanned twice a week between February 2021 and February 2022 with two breaks (Jun. to Oct. 2021, and Jan. 2022) where functional and structural MRI data (M. Y. Wang et al., 2024; M. Y. Wang et al., 2023a) were collected. In total, there are 38, 40, and 25 T1w MRI sessions for subjects 1, 2, and 3, respectively. The exact dates of these sessions can be found in **Table S1.**

All three participants speak at least two languages (their native languages, and English). Notably, the first participant has also been acquiring an additional language since January 2021 and remained COVID-19 free during the period of data collection. The second participant contracted COVID-19 around December 2021, while the third participant had COVID-19 in approximately August 2021.

Table1. Basic demographic information of subjects

	Sub1	**Sub2**	**Sub3**
Gender	Male	Male	Male
Age at baseline	31	27	40
Laterality	Right	Right	Right
Regular caffeine consumption?	No	Yes	Yes
Regular nicotine consumption?	No	No	No

2.2 Data collection

Data collection was embedded in the functional protocol of the BBSC project (M. Y. Wang et al., 2022, 2023a), which lasted around 25 minutes in total. The procedure of the data collection in the functional protocol is seven mins T1w MRI, 5 mins MR spectroscopy (MRS) data, and 12 mins rs-fMRI, where the data were collected with a 3T MRI scanner (GE Discovery MR750) with a 32-channel head coil at the Haukeland University Hospital in Bergen, Norway. The other modalities in the BBSC project have been described previously (Korbmacher et al., 2023; M. Y. Wang et al., 2024; M. Y. Wang et al., 2023b).

Seven-minute structural T1w images were acquired using a 3D Fast Spoiled Gradient-Recalled Echo (FSPGR) sequence with the following parameters: 188 contiguous slices acquired, with repetition time (TR) = 6.88 ms, echo time (TE) = 2.95 ms, flip angle (FA) = 12°, slice thickness = 1 mm, in-plane resolution = 1 mm × 1 mm, and field of view (FOV) = 256 mm, with an isotropic voxel size of 1 mm^3.

2.3 Data processing

Cortical thickness and surface area, as well as the cortical and subcortical volumes were computed with FreeSurfer v7.2 (freesurfer-darwin-macOS-7.2.0-20210713-aa8f76b) (Dale et al., 1999; Fischl et al., 1999). First, each session was processed with the cross-sectional *recon-all* stream. Then, the results went through the longitudinal stream (Reuter et al., 2012), where an unbiased within-subject template was created by using a robust, inverse consistent registration (Reuter, Rosas, & Fischl, 2010). For more details on data processing, see the **Supplementary Materials**.

It has become common practice to report brain imaging results in a common brain atlas (Desikan et al., 2006; Yeo et al., 2011) to aggregate or compare findings across different studies. Among these atlases, the Desikan- Killiany (DK) atlas (Desikan et al., 2006) has

become the most commonly used atlas in the T1w brain imaging studies (Bethlehem et al., 2022; Chen et al., 2012; L. T. Elliott et al., 2018; Genon et al., 2022; Grasby et al., 2020; Lemaitre et al., 2012; Vijayakumar et al., 2016). The DK atlas was developed based on curvature-based information such as the sulcal/gyral representations and contains 34 cortical brain regions in each hemisphere (Desikan et al., 2006). In this study, therefore, IDPs including the cortical thickness, surface area, and cortical brain volume were extracted from those 68 brain regions. Additionally, 7 subcortical regions (thalamus, pallidum, amygdala, hippocampus, putamen, accumbens area, and caudate nucleus) based on the *aseg* atlas were used for the subcortical brain volume analysis.

Moreover, the T1w images were quality assessed with MRIQC 23.1.0 (Esteban et al., 2017), where several image quality metrics (IQMs) were generated. Head movement was evaluated using coefficient of joint variation (CJV) values, which was proposed as a measure for INU correction algorithms. Higher CJV indicates head motion or INU artifacts, whereas lower values imply better image quality (Ganzetti, Wenderoth, & Mantini, 2016). From the data distribution of CJV, it is noticeable that there were two sessions (sessions 1 and 7) with excessive head movements in sub3. Accordingly, those two sessions were excluded from all analyses except the analyses on the effects of head movement. The IQMs is described with the image quality procedures in the **Supplementary Materials**.

2.4 Data Analysis

2.4.1 Coefficient of variation:

For each subject, stability was quantified with the coefficient of variation (CV), defined as the ratio of an estimate of variability and a mean, and it estimates the dispersion of the different measurement values to the average values (Brandmaier et al., 2018; M. Y. Wang et al., 2024). The CV values are always positive with smaller values indicating higher stability (Brandmaier et al., 2018; M. Y. Wang et al., 2024). We computed CVs as follows:

$$CV(\%) = \left(\frac{std}{mean}\right) * 100$$

where *std* denotes the standard deviation of the measurements taken across sessions for the same subject, while *mean* refers to the average of the within-subject measurements.

CVs facilitate the comparison of variability across varying units or scales (Brandmaier et al., 2018). It has also been instrumental in assessing the stability of measurements over time, where it is especially suitable for the within-subject design (Brandmaier et al., 2018; M. Y. Wang et al., 2024). Lower CVs indicate less variability relative to the mean, signifying higher stability or precision. Conversely, higher CVs indicate more variability relative to the mean, suggesting lower stability or precision (Brandmaier et al., 2018; M. Y. Wang et al., 2024).

2.4.2 Percentage change:

To account for discrepancies among different brain regions, the percentage changes instead of raw values of each IDP were used to illustrate the discrepancy (e.g. **Figs 2-5, 8**), which were calculated as the deviation from the mean divided by the mean itself. Furthermore, in order to explore which brain regions covaried, correlation matrices were computed within and between each phenotype.

2.4.3 Time-of-day & daylight length effects

Time-of-day was classified based on the data collection time, labeling sessions before noon as 'morning' and those after as 'afternoon'. The distribution of sessions was as follows: in sub1, there were 22 morning and 16 afternoon sessions; in sub2, 23 morning and 16 afternoon

sessions; and in sub3, 14 morning and 9 afternoon sessions. Daylight hour data, ranging from 120 to 948 minutes, was obtained from the weather station in the Florida area of Bergen maintained by the University of Bergen (https://veret.gfi.uib.no/). The time of day indices and daylight hours are described in **Table S1**.

Regarding the time-of-day and daylight-hour effects, to increase the statistical power, the effect size calculated within each subject will be aggregated using a meta-analysis (Viechtbauer, 2010). In addition, to explore whether the effect size is too trivial to be considered regardless of its significance from meta-analysis, equivalent tests will be implemented (Lakens, 2017; Lakens, Scheel, & Isager, 2018). The rationale of the equivalent test is straightforward: if the observed effect size of one factor is significantly different from a predefined effect size (i.e. 0.5), it then can be deduced that this effect size is too trivial (< 0.5), and the factor can be left out in future experiment designs (Lakens, 2017; Lakens et al., 2018; Vidal-Pineiro et al., 2021). Otherwise, it cannot be ruled out that there is no actual effect of that factor (Lakens, 2017; Lakens et al., 2018).

Accordingly, the following steps were implemented to evaluate the time-of-day effect and the daylight-hour effect on the IDPs. Here, for the sake of simplicity of the general linear model, the IDPs in this analysis only include the average cortical thickness, total surface area, and total cortical as well as subcortical brain volumes, instead of looking at the 64 regions separately.

First, the general linear model was fitted within each subject to examine the statistical significance of each subject, where the normalized values of each IDP were designated as dependent variables, and time of day or daylight hours were considered as the independent variables:

$$Normalized\ values = \beta_0 + \beta_1(time) + \epsilon,$$

where β_0 is the intercept; β_1 is the fixed effect coefficients for each predictor; *time* represents time of day or daylight hours, and □ is the residual error.

Second, the beta values and standard deviation errors (SE) derived from the linear model were fed into the *rma* function in the package Metafor (v4.6.0) (Viechtbauer, 2010) to aggregate estimates of the strength of the effects.

Third, the equivalence test was computed with the package TOSTER (V0.8.3) (Lakens, 2017; Lakens et al., 2018) based on the meta-analysis results to examine the practical significance meaning whether the effect was too trivial to ignore (Lakens, 2017; Lakens et al., 2018; Vidal-Pineiro et al., 2021). Here, we set the equivalence bounds for a median effect size of -0.50 and 0.50 at a type I error (alpha) of 0.05.

2.4.4 Head movement effect

To assess the influence of head movement on the stability of IDPs, paired *t*-tests were executed between the CV values of sessions before and after quality checking. Specifically, data from sub3 were used since two sessions were excluded because of the presence of excessive head movements.

2.4.5 Brain region size

In order to investigate the influence of different brain region sizes exerting on stability, the brain region sizes indicated by their volume and CVs were normalized within each subject and each hemisphere, leading to 204 (4*2*3) for thickness, surface area as well as cortical volume, and 42 (7*2*3) data points for subcortical volume. Then, Pearson's correlation between normalized brain region size and CVs was calculated.

Statistical analyses and visualizations were done with R 4.3.2 (R Core Team, 2022), and visualization was performed with ggplot2 (v3.5.1) (Wickham, 2009), ggseg (v1.6.6) (Mowinckel & Vidal-Piñeiro, 2020), and patchwork (v1.2.0).

3 Results

3.1 Longitudinal vs cross-sectional streams

The CVs of the longitudinal and cross-sectional processing streams on cortical brain volumes from FreeSurfer are described in **Table 2**. Meanwhile, the percentage changes against the average of different brain tissues for each subject are illustrated in **Fig. 1**.

As shown in **Table 2 and Fig. 1**, the CVs and percentage changes generated by the longitudinal processing stream are smaller than those of the cross-sectional stream, which indicates the longitudinal stream generates more stable results. Therefore, the following analyses were based on the results derived from the longitudinal processing stream.

Table 2. The longitudinal stream generates smaller CVs

	Sub1		**Sub2**		**Sub3**	
	Longitudinal	Cross-sectional	Longitudinal	Cross-sectional	Longitudinal	Cross-sectional
Total Brain	0.61	1.16	0.54	1.48	0.47	0.58
Gray Matter	0.81	1.06	0.71	1.86	0.94	1.02
Left - GM	0.89	1.17	0.80	1.97	1.10	1.14
Right - GM	0.91	1.13	0.74	1.84	0.90	1.03
White Matter	0.66	1.79	0.65	1.74	0.89	1.42
Left - WM	0.69	1.86	0.63	1.76	1.22	1.49
Right - WM	0.76	1.77	0.74	1.76	0.81	1.51

All CVs are reported as percentages, where smaller is better. Total Brain: '*BrainSegVolNotVent*' generated from FreeSurfer.

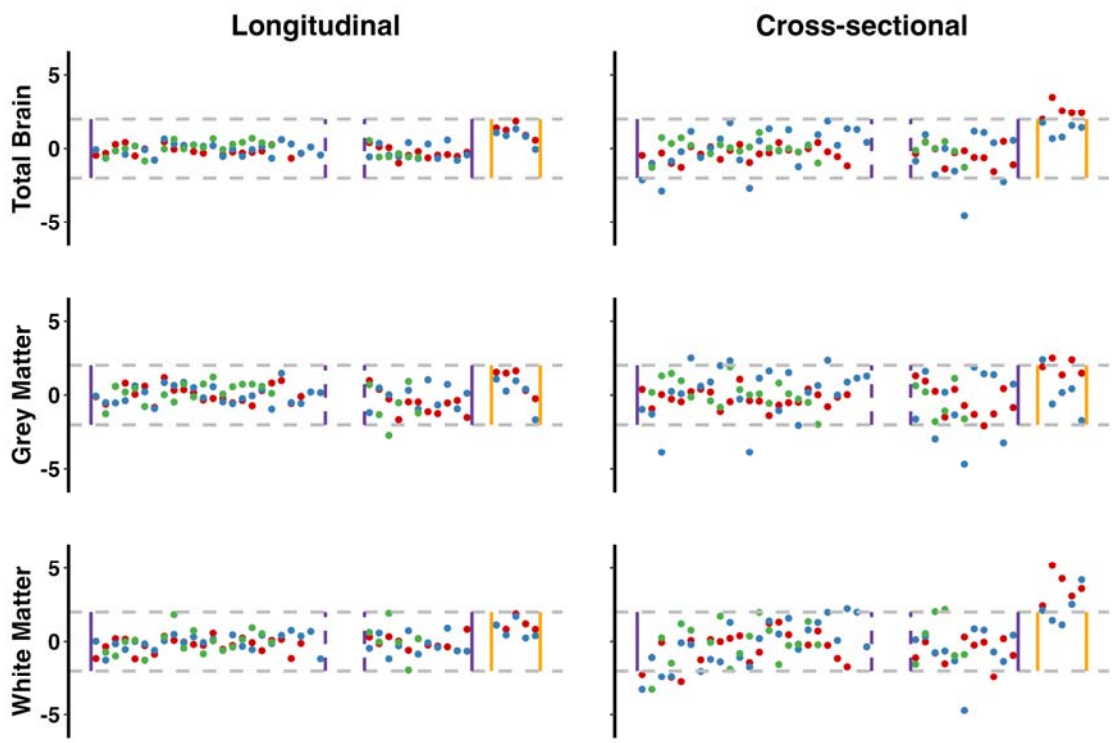

Fig. 1. Percentage changes of different brain volumes from different processing streams. Percentage changes along the data collections generated from the longitudinal and cross-sectional processing streams. The x-axis represents the time sequence of data collection while the y-axis depicts the percentage change. The purple solid vertical lines denote that the data were collected in the same year whereas the yellow solid vertical lines represent the data were collected the next year. In addition, the gap between the two dashed purple lines represents summer break while the gap between the purple and yellow solid lines indicates the winter break. The gray horizontal dashed lines denote 2% percentage changes. The red color represents subject 1, the blue depicts subject 2, and the green represents subject 3.

3.2 The stability of IDPs

3.2.1 Cortical thickness

The raw values (**Table S2**) and characteristics (**Fig. S2**) of cortical thickness have been described in the **Supplementary Materials**. The CVs of within-subject thickness ranged from 0.67 to 4.40 across all subjects, where most brain regions had CVs below 2. Specifically, the CVs vary from 0.74 to 2.64 for sub1, 0.67 to 3.24 for sub2, and 0.84 to 4.40 for sub3 (**Table 3**). Furthermore, the percentage changes in almost all brain regions across the three subjects were well-constrained within the 5% as illustrated in **Fig. 2.** Several brain regions, however, showed larger CVs and percentage changes across all three subjects (**Fig. 2** and **Table 3**), such as the temporal pole, frontal pole, pericalcarine, and entorhinal cortex.

Table 3. The CVs of the cortical thickness based on the DK atlas

	Sub1		**Sub2**		**Sub3**	
	Left	Right	Left	Right	Left	Right
transversetemporal	1.59	1.45	1.90	1.40	3.94	2.05
temporalpole	1.85	2.25	2.72	3.24	4.40	3.28
supramarginal	1.00	1.20	1.07	0.92	1.81	1.32

superiortemporal	0.76	0.74	0.98	0.85	0.92	1.30
superiorparietal	1.21	1.33	1.11	1.18	1.72	1.04
superiorfrontal	0.98	0.92	1.11	1.14	1.42	1.43
rostralmiddlefrontal	1.38	0.98	1.46	1.74	1.58	1.46
rostralanteriorcingulate	1.36	1.38	1.21	1.51	1.22	1.23
precuneus	1.33	1.09	1.12	1.00	1.28	1.15
precentral	0.92	1.06	1.11	1.05	2.22	1.16
posteriorcingulate	1.16	1.13	2.67	1.88	1.27	1.33
postcentral	0.91	0.97	1.20	1.13	2.26	1.25
pericalcarine	1.76	2.64	1.86	3.16	3.41	3.25
parstriangularis	1.07	1.18	1.66	1.41	2.22	1.91
parsorbitalis	1.24	1.35	2.07	1.97	2.60	1.81
parsopercularis	0.98	1.20	1.32	1.16	2.26	1.81
parahippocampal	0.95	0.99	1.18	1.76	1.58	1.77
paracentral	1.67	1.85	1.89	1.71	1.70	1.54
middletemporal	0.83	0.86	0.97	0.91	1.17	1.29
medialorbitofrontal	2.39	1.77	1.70	1.31	1.48	1.44
lingual	1.16	1.14	1.12	1.62	1.06	2.14
lateralorbitofrontal	1.23	1.36	1.67	1.33	2.14	1.91
lateraloccipital	1.25	1.05	1.36	1.04	1.28	1.34
isthmuscingulate	1.48	1.75	1.04	1.16	1.25	1.24
insula	1.16	1.15	1.09	1.20	1.64	1.38
inferiortemporal	1.10	0.88	1.09	0.72	1.22	1.10
inferiorparietal	1.56	1.95	1.05	1.16	1.71	1.23
fusiform	1.08	0.80	0.85	0.67	1.12	0.84
frontalpole	2.28	2.11	2.94	2.14	1.30	2.87
entorhinal	2.03	1.55	2.19	2.43	3.16	1.60
cuneus	1.51	2.02	1.62	1.47	1.88	2.27
caudalmiddlefrontal	1.69	1.23	1.36	1.45	1.88	1.41
caudalanteriorcingulate	1.62	1.44	1.86	1.34	1.44	1.76
bankssts	0.93	1.88	1.17	1.17	2.07	1.23
average	0.72	0.66	0.68	0.68	0.95	0.83

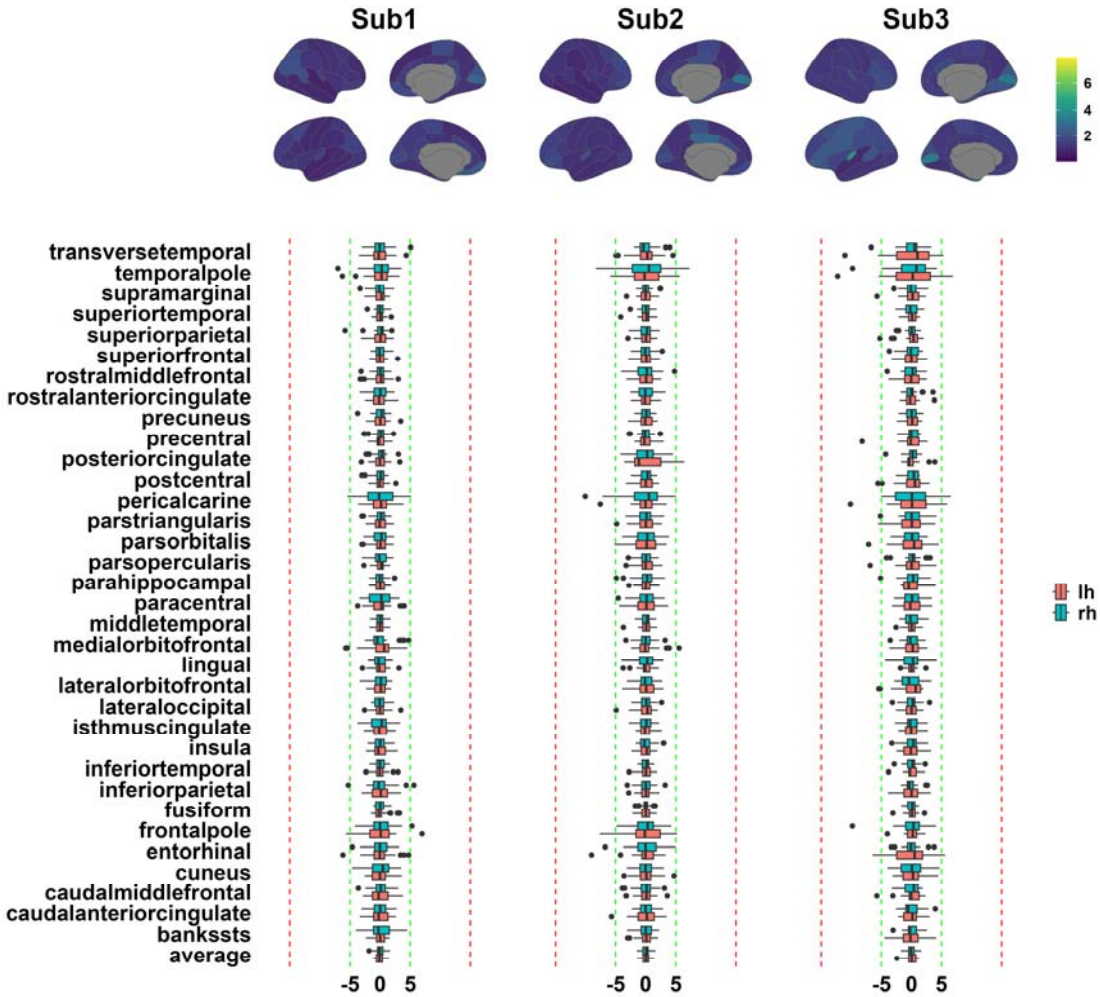

Fig. 2. The CVs and percentage changes in the cortical thickness. The upper panel depicts the coefficient of the variation (CV) for each subject. The lower boxplots show percentage change against the average for each brain region and each subject. The green lines are in the range of ±5 % while the red lines depict the range of ±15%. All values in the boxplot are given as percentages.

3.2.2 Surface area

The raw values (**Table S3**) and characteristics (**Fig. S4**) of the surface area have been described in the **Supplementary Materials**. The CVs of the within-subject area ranged from 0.41 to 7.25, specifically 0.41 to 4.52 for Sub1, 0.49 to 7.25 for Sub2, and 0.53 to 5.34 for Sub3 (**Table 4**). Subject 2 manifested a generally larger percentage change in the cingulate cortex (**Fig. 3**) and greater CVs (**Table 4**) than other brain regions along the data collections. Aside from the cingulate cortex in sub2, almost all brain regions showed percentage changes within 5% across all three subjects (**Fig. 3**). Notably, several surface areas showed larger CVs and percentage changes across all three subjects, including the temporal pole, frontal pole, and entorhinal cortex (**Fig. 3** and **Table 4**).

Table 4. The CVs of the surface area based on the DK atlas

	Sub1		**Sub2**		**Sub3**	
	Left	Right	Left	Right	Left	Right

transversetemporal	1.56	1.77	1.99	2.26	3.42	1.91
temporalpole	3.50	4.83	4.58	4.01	4.81	5.13
supramarginal	0.61	0.65	0.63	0.82	0.53	0.74
superiortemporal	0.59	0.40	0.73	0.64	0.90	0.73
superiorparietal	0.72	0.59	0.82	0.92	0.91	0.91
superiorfrontal	0.56	0.55	0.76	0.76	0.88	0.91
rostralmiddlefrontal	1.10	1.24	1.01	1.21	1.05	0.92
rostralanteriorcingulate	1.46	2.24	2.15	2.27	1.83	1.80
precuneus	0.46	0.52	0.68	0.67	0.83	0.77
precentral	0.81	0.76	1.06	0.80	1.24	0.89
posteriorcingulate	1.18	1.24	7.25	6.94	1.29	1.54
postcentral	0.97	0.77	1.11	1.04	1.95	1.01
pericalcarine	1.38	0.94	1.70	1.11	1.13	1.43
parstriangularis	1.57	0.79	1.39	1.15	1.15	0.86
parsorbitalis	2.04	1.51	1.86	1.43	2.05	1.49
parsopercularis	0.91	0.39	0.77	0.98	1.24	1.05
parahippocampal	1.25	1.47	1.14	1.29	1.17	1.03
paracentral	0.78	1.03	1.52	1.31	1.56	1.23
middletemporal	1.22	1.66	0.86	0.78	0.95	0.80
medialorbitofrontal	4.52	0.99	2.09	1.61	1.44	1.27
lingual	1.39	1.30	1.50	1.65	1.33	2.01
lateralorbitofrontal	0.97	1.13	1.57	1.76	1.96	2.27
lateraloccipital	0.86	0.80	1.06	0.86	0.92	1.23
isthmuscingulate	1.60	2.46	1.23	1.53	1.05	1.41
insula	0.76	1.14	1.56	2.84	1.44	1.16
inferiortemporal	0.53	0.85	1.11	0.77	1.25	1.04
inferiorparietal	0.79	0.90	0.91	0.82	0.74	0.66
fusiform	0.95	0.89	1.08	1.34	1.23	0.87
frontalpole	3.20	3.80	1.98	1.95	2.15	3.80
entorhinal	2.84	2.59	4.33	2.84	5.34	3.26
cuneus	1.64	1.92	1.40	1.94	1.99	2.37
caudalmiddlefrontal	0.58	0.55	0.77	1.29	1.11	1.08
caudalanteriorcingulate	0.64	1.93	4.38	2.28	1.18	2.17
bankssts	0.41	0.88	0.49	0.77	0.65	0.85
Total	0.52	0.55	0.67	0.74	0.67	0.58

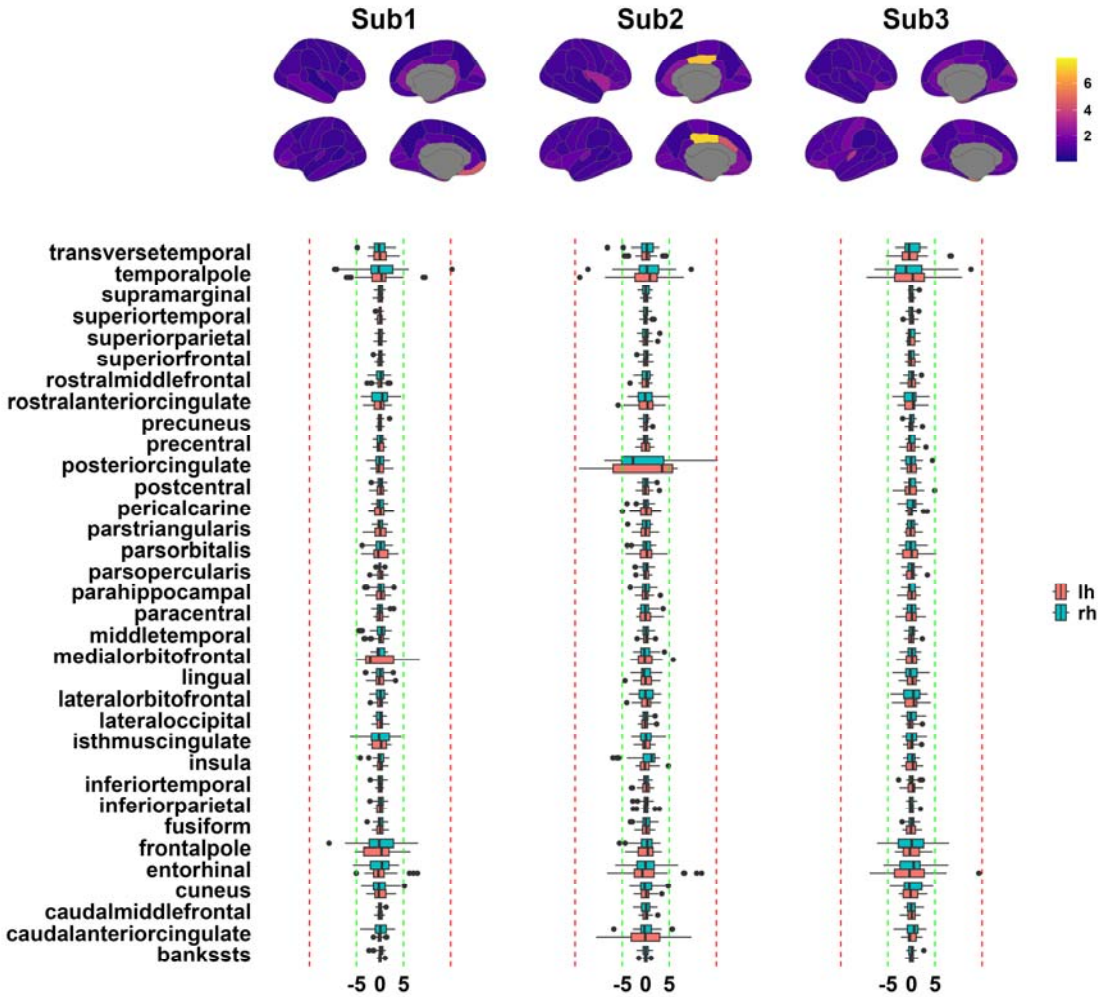

Fig. 3 The CVs and percentage changes in surface area. The upper panel depicts the coefficient of variation (CV) for each subject. The lower boxplot shows percentage changes for each brain region and each subject. The green lines are in the range of ±5 % while the red lines depict the range of ±15%. The unit of all values in the boxplot is percentage.

3.2.3 Cortical brain volume

The raw values (**Tables S4 & S5**) and characteristics (**Fig. S6**) of the cortical brain volume are described in the **Supplementary Materials**. The CVs of the within-subject brain volume range from 0.64 to 4.73 for sub1, 0.72 to 4.87 for sub2, and 0.86 to 4.99 for sub3 (**Table 5**). Furthermore, several brain regions showed larger CVs (**Table 5**) and percentage changes (**Fig. 4**), such as the temporal pole, pericalcarine, and entorhinal cortex. Moreover, aside from the abovementioned regions, the percentage changes are well confined within 5% in all subjects (**Fig. 4**).

Table 5. The CVs of the cortical brain volume based on the DK atlas

	Sub1		**Sub2**		**Sub3**	
	Left	Right	Left	Right	Left	Right
transversetemporal	1.51	1.63	1.43	1.29	2.98	1.85
temporalpole	1.96	1.99	2.63	2.96	4.99	2.96

supramarginal	1.04	1.30	0.98	0.96	1.67	1.06
superiortemporal	0.95	1.01	1.15	0.83	0.98	1.06
superiorparietal	1.36	1.49	1.55	1.64	1.62	0.86
superiorfrontal	1.05	1.10	1.20	1.08	1.59	1.31
rostralmiddlefrontal	1.27	1.31	1.34	1.46	1.58	1.70
rostralanteriorcingulate	1.26	1.31	1.75	1.07	1.39	1.03
precuneus	1.34	1.14	1.28	1.07	1.34	1.09
precentral	1.45	1.32	1.66	1.37	2.09	1.00
posteriorcingulate	1.05	1.20	4.83	4.87	1.92	1.00
postcentral	1.58	1.45	1.44	1.98	1.87	1.08
pericalcarine	1.83	3.54	2.20	3.94	4.05	4.12
parstriangularis	1.03	1.43	1.29	1.09	1.91	1.87
parsorbitalis	1.47	0.98	2.13	1.81	1.95	1.78
parsopercularis	1.21	1.28	1.30	1.11	1.94	1.82
parahippocampal	1.38	1.51	1.69	1.53	1.81	1.92
paracentral	1.77	1.70	2.00	2.14	1.70	1.39
middletemporal	1.01	1.90	1.03	0.78	1.17	1.44
medialorbitofrontal	4.73	2.63	2.71	1.62	1.85	1.47
lingual	1.08	1.19	1.27	1.54	1.02	1.63
lateralorbitofrontal	1.05	1.24	1.31	1.07	1.63	1.74
lateraloccipital	1.38	0.93	1.18	1.23	1.44	1.53
isthmuscingulate	1.12	1.40	1.13	1.62	1.12	1.45
insula	1.19	1.33	1.17	1.64	2.00	1.23
inferiortemporal	1.42	1.13	1.09	0.89	1.37	1.19
inferiorparietal	1.15	1.51	1.11	1.13	1.50	1.07
fusiform	1.31	0.64	0.89	0.72	0.95	0.90
frontalpole	1.87	1.73	1.67	1.32	1.44	2.20
entorhinal	2.88	2.22	2.42	3.74	3.36	3.09
cuneus	1.25	1.90	1.55	3.26	1.47	1.55
caudalmiddlefrontal	1.95	1.66	1.98	2.16	2.02	1.37
caudalanteriorcingulate	1.49	1.23	3.76	1.85	1.69	1.40
bankssts	0.77	1.84	1.03	0.98	1.55	1.28

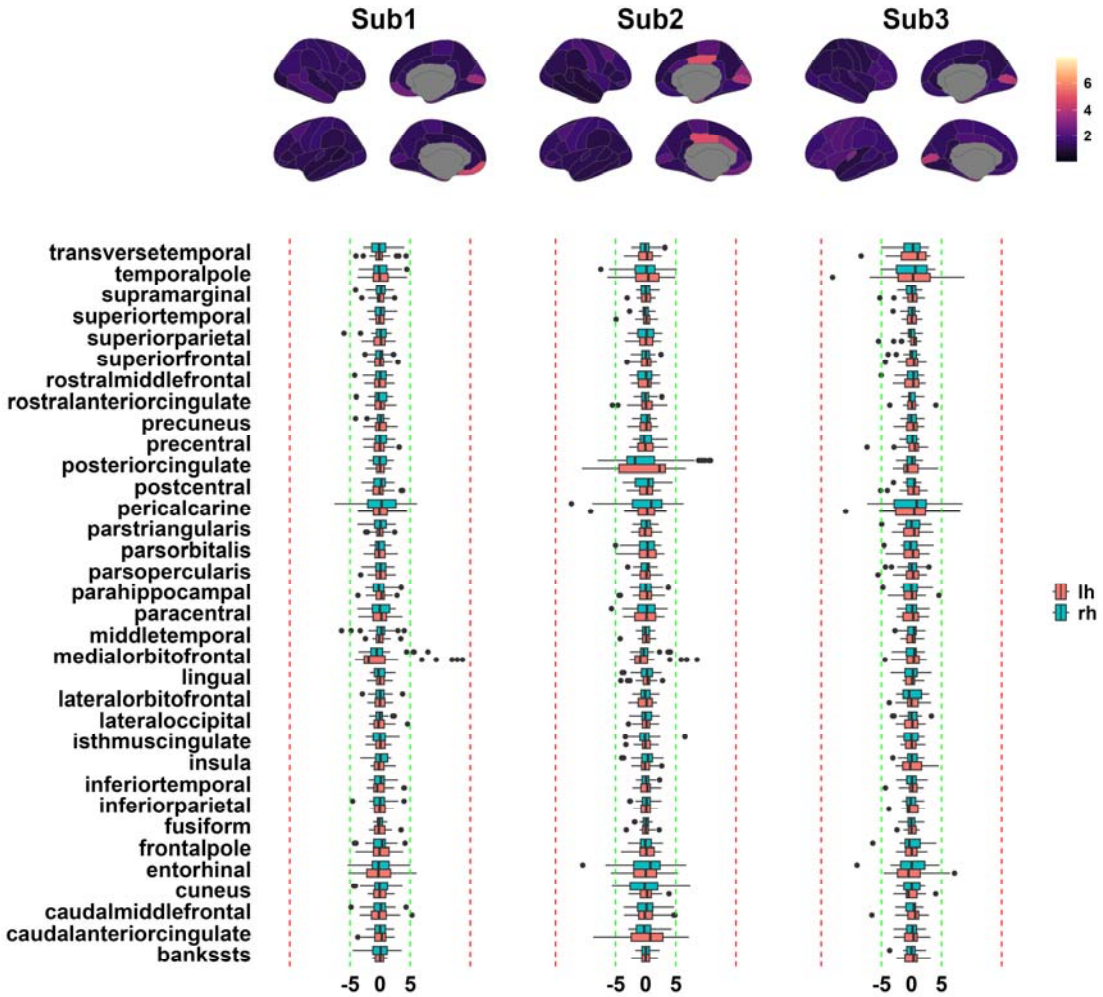

Fig. 4. The CVs and percentage changes in cortical brain volume. The upper panel depicts the coefficient of variation (CV) for each subject. The lower boxplot shows the percentage change for each brain region and subject. The green lines are in the range of ±5 % while the red lines depict the range of ±15%. All values in the boxplot are reported as percentages.

3.2.4 Subcortical brain volume

The raw values (**Table S6**) and characteristics (**Fig. S9**) of the subcortical brain volumes are described in the **Supplementary Materials**. The CVs of the within-subject subcortex ranged from 0.64 to 6.17 for Sub1, 0.54 to 6.24 for Sub2, and 0.51 to 7.03 for Sub3 (**Table 6**). As depicted in the upper panel of **Fig. 5**, the subcortex including the thalamus, caudate, putamen, pallidum, hippocampus, and amygdala, showed very small CVs (< 2.5%) except the accumbens area (**Table 6**), especially the left side. In addition, **Table S7** depicts the CVs of the subcortices along with the cerebellum, ventricles, brain stem, corpus callosum (CC), and CSF, where it is shown that the corpus callosum showed much higher stability as a whole than its parts such as the anterior, middle, and posterior (**Fig. S11**).

Table 6. The CVs of the non-cortical brain volume based on the DK atlas

	Sub1		Sub2		Sub3	
	Left	Right	Left	Right	Left	Right

Thalamus	1.04	1.39	0.70	1.24	1.01	1.12
Caudate	1.12	1.14	1.38	0.88	0.90	0.86
Putamen	0.70	1.16	1.20	1.22	1.34	1.43
Pallidum	1.14	1.28	1.33	1.32	1.19	1.52
Hippocampus	0.93	0.71	0.95	1.15	1.19	1.02
Amygdala	1.61	1.48	2.43	1.43	1.60	1.81
Accumbens-area	6.17	2.36	6.24	2.69	7.03	3.00
Total	0.46	0.72	0.51	0.64	0.59	0.51

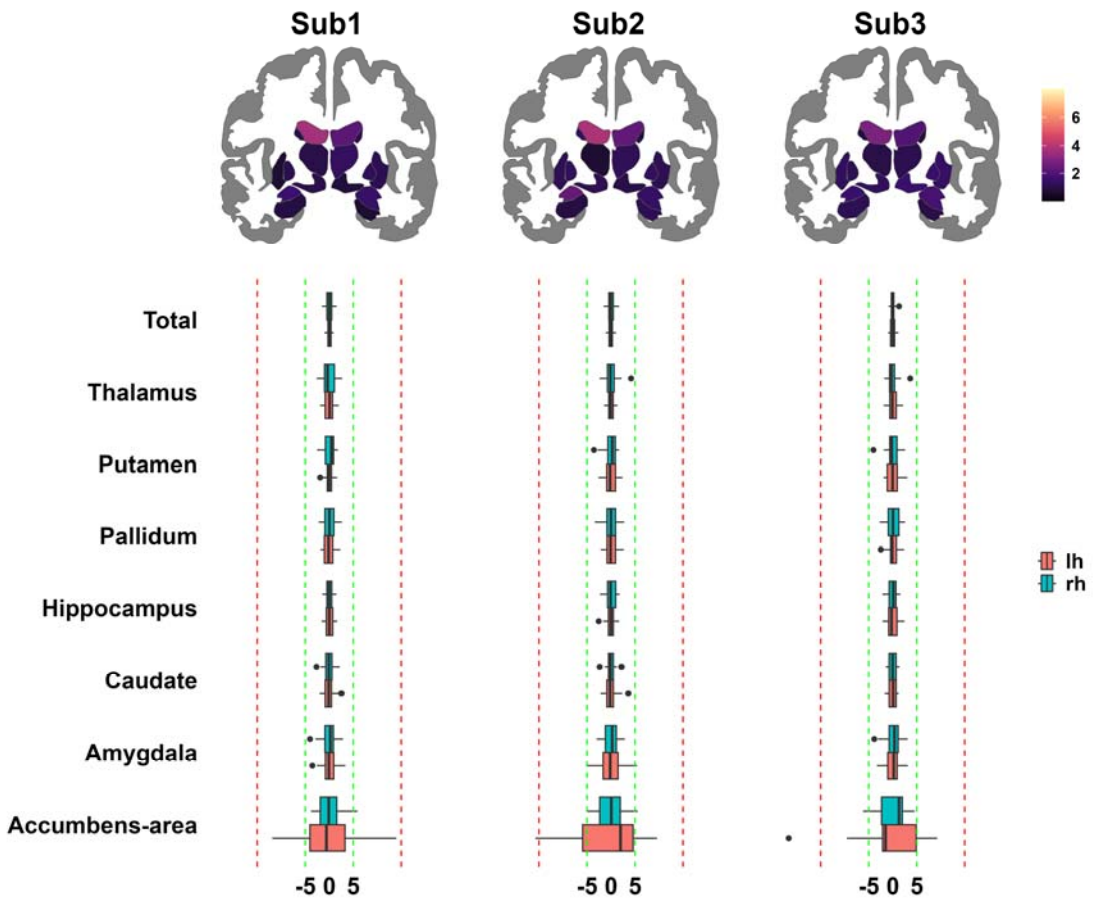

Fig. 5. CVs and percentage change in brain volume. The upper panel depicts the coefficient of variation (CV) for each subject. The lower boxplots show the percentage change for each brain region and each subject. The green lines are in the range of ±5 % while the red lines depict the range of ±15%. All values in the boxplots are reported as percentages.

3.2.5 Correlation of percentage changes within and between different phenotypes

Within phenotypes, the average correlation coefficients of thickness (**Fig. 6A**), area (**Fig. 6B**), and volume (**Fig. 6C**) were 0.25, 0.23, and 0.27, respectively. Moreover, between phenotypes, the average correlation coefficients (without the diagonal lines) of thickness-volume (**Fig. 6D**), thickness-area (**Fig. 6E**), and area-volume (**Fig. 6F**) were 0.26, -0.09, and -3.4×10^{-4}, respectively. More importantly, the correlation coefficients between brain regions (the

diagonal lines in **Fig. 6DEF**) are positive for thickness-volume, negative for thickness-area, and negligible for area-volume (**Table 7**). The distribution of correlation coefficients of each phenotype association is depicted in **Fig. S12**.

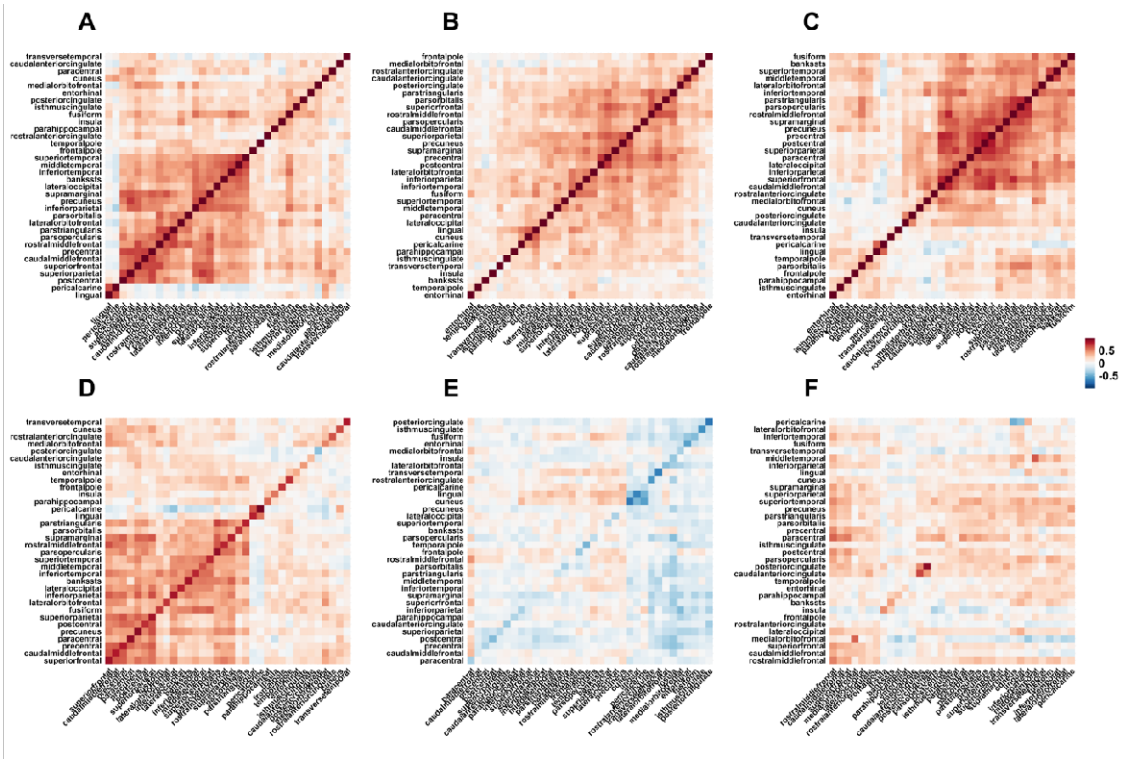

Fig. 6. Correlation matrices within and between different phenotypes. Correlation matrices for **(A)** Thickness, **(B)** Surface area, **(C)** Brain volume, **(D)** Thickness and volume, **(E)** Thickness and area, and **(F)** Area and volume.

Table 7. The correlation coefficients across different phenotypes

	Thickness-Volume	Thickness-Area	Area-Volume
pericalcarine	0.96	-0.22	-0.02
precuneus	0.91	-0.48	-0.18
parsopercularis	0.90	-0.20	0.11
paracentral	0.89	-0.62	-0.27
inferiortemporal	0.87	-0.02	0.14
inferiorparietal	0.87	-0.57	-0.28
bankssts	0.87	-0.10	0.20
transversetemporal	0.84	-0.77	-0.38
superiorparietal	0.83	-0.66	-0.23
lateraloccipital	0.82	-0.49	-0.06
superiorfrontal	0.82	-0.41	0.11
superiortemporal	0.80	-0.51	-0.04
supramarginal	0.80	-0.43	0.04
caudalmiddlefrontal	0.79	-0.24	0.18

lingual	0.78	-0.65	-0.13
fusiform	0.78	-0.23	0.26
parstriangularis	0.77	-0.37	0.09
precentral	0.77	-0.59	-0.01
middletemporal	0.76	-0.22	0.35
lateralorbitofrontal	0.76	-0.36	0.01
rostralmiddlefrontal	0.76	-0.07	0.45
temporalpole	0.74	-0.45	-0.06
frontalpole	0.73	-050	-0.13
postcentral	0.72	-0.55	0.11
parsorbitalis	0.69	-0.31	0.32
parahippocampal	0.67	-0.22	0.28
cuneus	0.65	-0.70	-0.04
rostralanteriorcingulate	0.62	-0.59	0.07
insula	0.60	-0.35	0.44
medialorbitofrontal	0.50	-0.31	0.59
isthmuscingulate	0.46	-0.63	0.18
entorhinal	0.43	-0.51	0.22
caudalanteriorcingulate	0.33	-0.36	0.65
posteriorcingulate	-0.35	-0.70	0.88

3.3 The influence of the stability

Regarding the time-of-day and daylight-hour effects, the meta-analysis can tell us about the significance characters of this specific dataset while the equivalent test can tell us about the generalization of our results by indicating whether the observed effect size is comparable to a predefined effect size (i.e. 0.5) (Lakens, 2017; Lakens et al., 2018).

The meta-analysis and equivalence test results of the time-of-day and daylight-hour effects are depicted in **Fig. 7**. The square dots represented the effect size estimated from this study where the extended lines illustrated the 90% (bold lines) and 95 % (narrow lines) confidence intervals (CI). If the CIs did not cross the zero lines, it means the meta-analysis results are significant from 0. Moreover, if the CIs did not cross the ± 0.5 lines, it means the equivalence analysis results are significant meaning the results are trivial or can be practically ignored (Lakens, 2017; Lakens et al., 2018).

3.3.1 Time-of-day effect

The distributions of percentage change for morning and afternoon sessions of each brain region for each IDP were depicted in **Figs S3, S5, S7, S8**, and **S10.**

Thickness (average): the significant time-of-day (ToD) effect can be observed in sub1 (β = 0.63, p = 0.006, SE = 0.22), but not in sub2 (β = 0.001, p = 0.996, SE = 0.23), and sub3 (β = -0.11, p = 0.72, SE = 0.31). Collectively, meta-analysis suggests that there is no significant ToD effect (β = 0.196, p = 0.40, SE = 0.24, CI 95% = [-0.26 0.66]). However, we cannot rule out there is no ToD effect based on the equivalence test (Z = -1.29, p = 0.099).

Surface area (total): no ToD effects were shown in sub1 (β = 0.04, p = 0.87, SE = 0.23), sub2 (β = -0.06, p = 0.80, SE = 0.23), and sub3 (β = 0.45, p = 0.14, SE = 0.30). Jointly, the meta-analysis (β = 0.096, p = 0.51, SE = 0.14, CI 95% = [-0.19 0.38]) and equivalence test (Z = -2.82, $p = 2.43 \times 10^{-3}$) also illustrated that there is no ToD effect.

Cortical volume (total): nonsignificant ToD effects were observed for sub1 (β = 0.39, p = 0.09, SE = 0.23), sub2 (β = 0.06, p = 0.80, SE = 0.23), and sub3 (β = 0.11, p = 0.71, SE = 0.31). Furthermore, the meta-analysis (β = 0.199, p = 0.17, SE = 0.14, CI 95% = [-0.08 0.48]) and the equivalence test (Z = -2.10, p = 0.02) corroborate the none ToD effect.

Subcortical volume(total): sub2 showed significant ToD effect (β = 0.93, p = 0.003, SE = 0.29), but not for sub1 (β = 0.09, p = 0.79, SE = 0.33) and sub3 (β = 0.28, p = 0.52, SE = 0.43). Although the meta-analysis demonstrated that there is no ToD effect (β = 0.47, p = 0.10, SE = 0.28, CI 95% = [-0.08 0.48]), the equivalence test suggested that the ToD effect cannot be ruled out (Z = -0.11, p = 0.46).

3.3.2 Daylight-hour effect

The distributions of percentage change along the daylight hour of each phenotype were depicted in **Figs S2D, S4D,** and **S6D.**

Thickness (average): no significant effects were found in sub1 (β = -0.003, p = 0.77, SE = 0.12), sub2 (β = -0.007, p = 0.53, SE = 0.11), and sub3 (β = 0.25, p = 0.10, SE = 0.14). The meta-analysis (β = 0.03, p = 0.82, SE = 0.09, CI 95% = [-0.15 0.20]) and the equivalence test (Z = -5.26, $p = 7.39 \times 10^{-8}$) reconfirm the non-significant effect.

Surface area (total): a significant effect was found in sub3 (β = 0.30, p = 0.04, SE = 0.14), but not in sub1 (β = 0.15, p = 0.21, SE = 0.11), and sub2 (β = 0.19, p = 0.097, SE = 0.11). The meta-analysis demonstrated that there was a significant effect (β = 0.20, p = 0.004, SE = 0.07, CI 95% = 0.06 0.34]), however, the equivalence test showed that the effect can be ignored since it was too small (Z = -4.31, $p = 8.31 \times 10^{-6}$)

Cortical volume (total): the significant effect was found in sub3 (β = 0.44, p = 0.002, SE = 0.13) but not for sub1 (β = 0.12, p = 0.30, SE = 0.12), for sub2 (β = 0.003, p = 0.77, SE = 0.11). The meta-analysis (β = 0.19, p = 0.11, SE = 0.12, CI 95% = [-0.04 0.42]) and the equivalence test (Z = -2.69, $p = 3.62 \times 10^{-3}$) suggested that the effect was nonsignificant.

Subcortical volume (total): a significant effect was found for sub3 ($\beta = 8.79 \times 10^{-4}$, $p = 1.33 \times 10^{-3}$, $SE = 2.38 \times 10^{-4}$), but not for sub1 ($\beta = -7.36 \times 10^{-5}$, p = 0.80, $SE = 2.93 \times 10^{-4}$), and sub2 ($\beta = -4.41 \times 10^{-4}$, p = 0.13, $SE = 2.88 \times 10^{-4}$). Although the meta-analysis demonstrated a non-significant effect ($\beta = 1.36 \times 10^{-4}$, p = 0.73, $SE = 4.01 \times 10^{-4}$, CI 95% = [-6.49×10^{-4} 9.21×10^{-4}]), the daylight-hour effect cannot be ruled out based on the equivalence test result (Z = -1.49, p = 0.07).

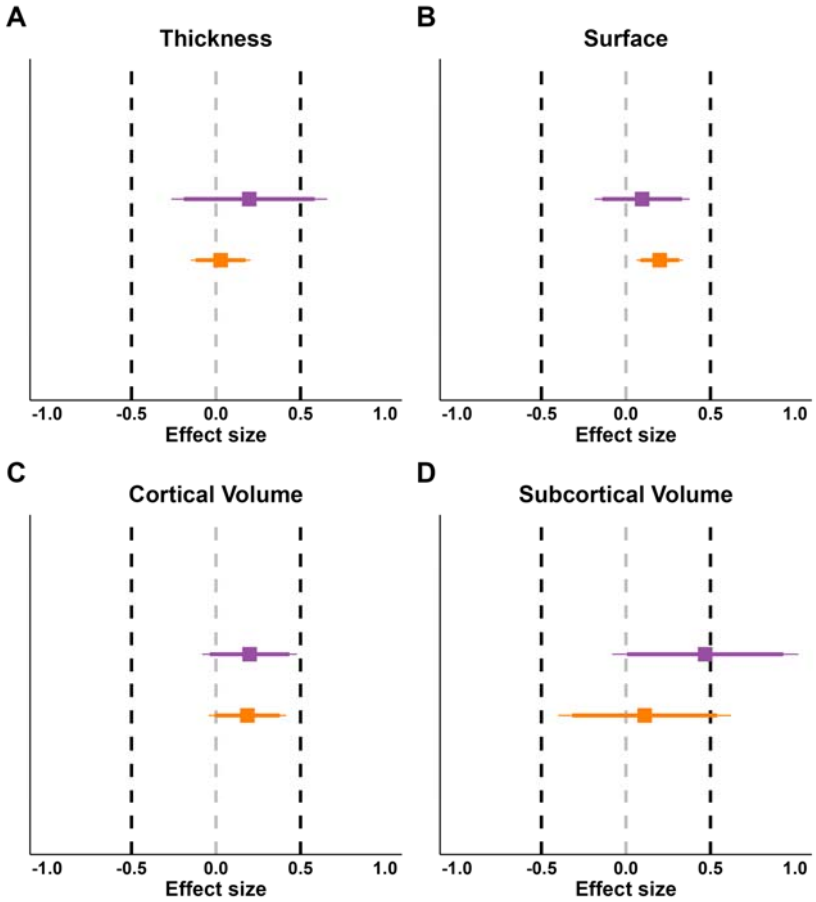

Fig. 7. The meta-analysis and equivalence test results of the time-of-day and daylight-hour effects. (A) Average brain thickness. **(B)** Total surface area. **(C)** Total cortical brain volume. **(D)** Total subcortical brain volume (summary of the thalamus, pallidum, amygdala, hippocampus, putamen, accumbens area, and caudate nucleus). The square dots represented the effect size estimated from this study where the extended lines illustrated the 90% (bold lines) and 95 % (narrow lines) CI. Purple and yellow colors represent the time-of-day and daylight-hour effects, respectively.

3.3.3 Head movement effect

In sub3, two sessions with excessive head motion indicated by the CJV (sessions 1 and 7) were excluded in the previous analyses. In order to investigate the head movement effect, CVs were calculated when considering the two excluded sessions in comparison to CVs without the two sessions. Paired t-tests were then used to compare those two CVs.

The CVs (**Table 8**) and percentage changes (**Fig. 8**) significantly improved after excluding those two sessions for the cortical thickness (left hemisphere: t_{33} = -7.6, $p = 4.8 \times 10^{-9}$, *Cohen's d* = 1.3; right hemisphere: t_{33} = -7.13, $p = 1.8 \times 10^{-8}$, *Cohen's d* = 1.22), surface area (left: t_{33} = -6.03, $p = 4.4 \times 10^{-7}$, *Cohen's d* = 1.03; right: t_{33} = -2.27, $p = 7.9 \times 10^{-5}$, *Cohen's d* = 0.73), and cortical brain volumes (left: t_{33} = -5.06, $p = 7.6 \times 10^{-6}$, *Cohen's d* = 0.87; right: t_{33} = -6.21, $p = 2.6 \times 10^{-7}$, *Cohen's d* = 1.06).

Table 8. The CVs of the cortical thickness based on the DK atlas

	Thickness				**Surface area**				**Cortical volume**			
	Left	Left_qc	Right	Right_qc	Left	Left_qc	Right	Right_qc	Left	Left_qc	Right	Right_qc

transversetemporal	4.61	3.94	3.43	2.05	4.04	3.42	4.04	1.91	3.57	2.98	2.26	1.85
temporalpole	4.71	4.40	3.26	3.28	4.72	4.81	5.04	5.13	4.96	4.99	3.31	2.96
supramarginal	2.45	1.81	1.91	1.32	1.40	0.53	1.16	0.74	1.86	1.67	1.42	1.06
superiortemporal	1.77	0.92	2.31	1.30	1.38	0.90	0.99	0.73	1.16	0.98	1.65	1.06
superiorparietal	2.64	1.72	2.97	1.04	2.79	0.91	2.76	0.91	1.89	1.62	1.77	0.86
superiorfrontal	1.78	1.42	2.19	1.43	1.54	0.88	1.59	0.91	1.56	1.59	1.48	1.31
rostralmiddlefrontal	2.35	1.58	1.74	1.46	1.36	1.05	1.03	0.92	1.67	1.58	1.71	1.70
rostralanteriorcingulate	1.35	1.22	1.47	1.23	2.38	1.83	2.06	1.80	1.34	1.39	1.03	1.03
precuneus	1.90	1.28	2.66	1.15	1.58	0.83	1.82	0.77	1.66	1.34	1.99	1.09
precentral	3.20	2.22	1.61	1.16	2.60	1.24	1.75	0.89	2.27	2.09	1.02	1.00
posteriorcingulate	1.62	1.27	1.78	1.33	1.42	1.29	1.78	1.54	1.97	1.92	1.35	1.00
postcentral	2.52	2.26	1.90	1.25	2.93	1.95	1.37	1.01	1.87	1.87	1.41	1.08
pericalcarine	3.43	3.41	3.16	3.25	2.31	1.13	1.39	1.43	3.99	4.05	3.95	4.12
parstriangularis	2.80	2.22	2.02	1.91	2.37	1.15	1.10	0.86	1.97	1.91	1.87	1.87
parsorbitalis	2.62	2.60	1.74	1.81	2.24	2.05	2.53	1.49	1.87	1.95	2.08	1.78
parsopercularis	2.64	2.26	2.18	1.81	1.33	1.24	1.25	1.05	2.32	1.94	2.31	1.82
parahippocampal	2.63	1.58	2.55	1.77	1.70	1.17	1.61	1.03	2.23	1.81	2.63	1.92
paracentral	3.43	1.70	2.97	1.54	2.98	1.56	2.65	1.23	2.55	1.70	2.03	1.39
middletemporal	2.65	1.17	2.67	1.29	1.30	0.95	0.97	0.80	1.90	1.17	2.30	1.44
medialorbitofrontal	1.51	1.48	1.63	1.44	1.44	1.44	1.23	1.27	1.90	1.85	1.57	1.47
lingual	1.39	1.06	2.09	2.14	1.53	1.33	1.99	2.01	1.22	1.02	1.61	1.63
lateralorbitofrontal	2.24	2.14	2.63	1.91	2.38	1.96	2.26	2.27	1.73	1.63	3.04	1.74
lateraloccipital	1.98	1.28	2.06	1.34	1.26	0.92	1.89	1.23	2.02	1.44	2.06	1.53
isthmuscingulate	1.65	1.25	1.30	1.24	1.56	1.05	1.41	1.41	1.44	1.12	1.39	1.45
insula	2.04	1.64	1.73	1.38	1.46	1.44	1.14	1.16	2.34	2.00	1.51	1.23
inferiortemporal	2.32	1.22	2.49	1.10	1.23	1.25	1.13	1.04	2.33	1.37	2.77	1.19
inferiorparietal	3.17	1.71	2.17	1.23	2.20	0.74	1.21	0.66	2.20	1.50	1.62	1.07
fusiform	1.53	1.12	1.59	0.84	1.37	1.23	0.91	0.87	1.41	0.95	1.57	0.90
frontalpole	1.83	1.30	4.01	2.87	2.99	2.15	5.77	3.80	1.56	1.44	2.45	2.20
entorhinal	3.59	3.16	2.49	1.60	5.26	5.34	3.29	3.26	3.35	3.36	3.79	3.09
cuneus	1.91	1.88	2.27	2.27	2.30	1.99	2.31	2.37	1.45	1.47	1.71	1.55
caudalmiddlefrontal	2.04	1.88	1.92	1.41	1.12	1.11	1.29	1.08	2.00	2.02	1.54	1.37
caudalanteriorcingulate	1.77	1.44	2.06	1.76	1.54	1.18	2.10	2.17	1.80	1.69	1.54	1.40
bankssts	3.14	2.07	2.12	1.23	0.65	0.65	0.95	0.85	2.40	1.55	2.26	1.28

Percentage CVs after excluding the two sessions with excessive head motion.

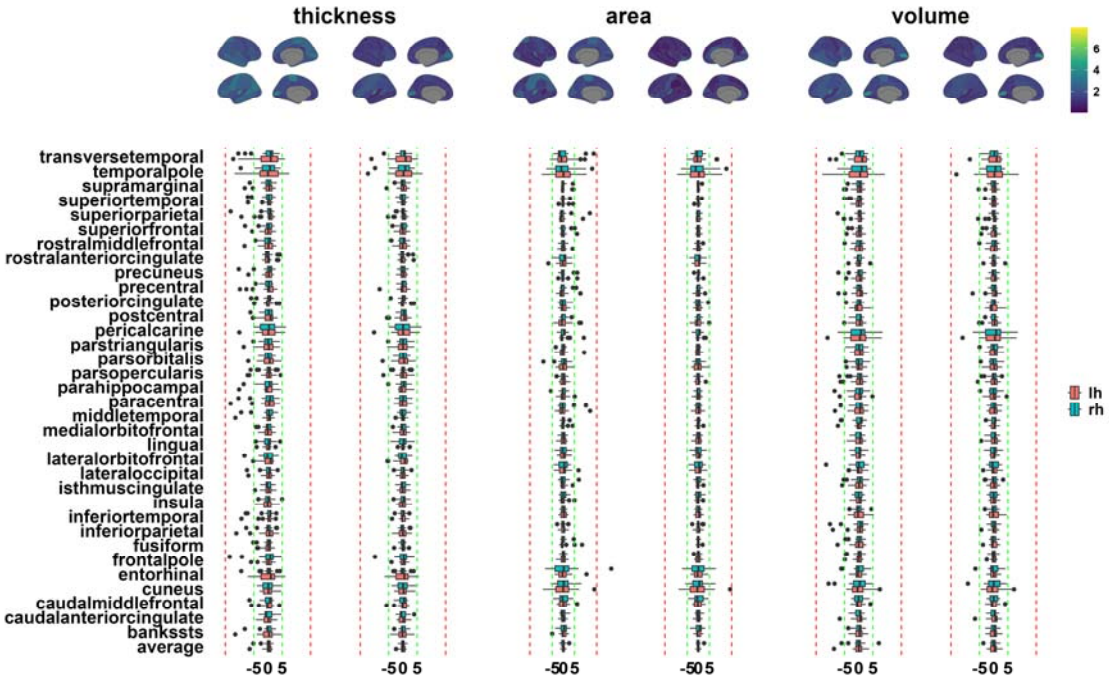

Fig. 8 The CVs and percentage changes before and after excluding two sessions with excessive head movement in sub3. The upper panels depicted the CVs for cortical thickness, surface area, and cortical brain volume. The bottom panels illustrate the percentage changes in each brain region for cortical thickness, surface area, and cortical brain volume. Under each IDP, the left sides were results from all sessions whereas the right sides were results from sessions excluding the two sessions.

3.3.4 Brain region size

As shown in **Fig. 9**, all IDPs CVs were significantly negatively correlated with their brain region size: thickness (r = -0.48, t_{202} = -7.84, $p = 2.62 \times 10^{-13}$, CI 95% = [-0.58 -0.37]); surface area (r = -0.45, t_{202} = -7.26, $p = 8.13 \times 10^{-12}$, CI 95% = [-0.56 -0.34]); cortical volume (r = -0.37, t_{202} = -5.68, $p = 4.71 \times 10^{-8}$, CI 95% = [-0.48 -0.25]); subcortical volume (r = -0.52, t_{202} = -3.83, $p = 4.40 \times 10^{-4}$, CI 95% = [-0.71 -0.25]).

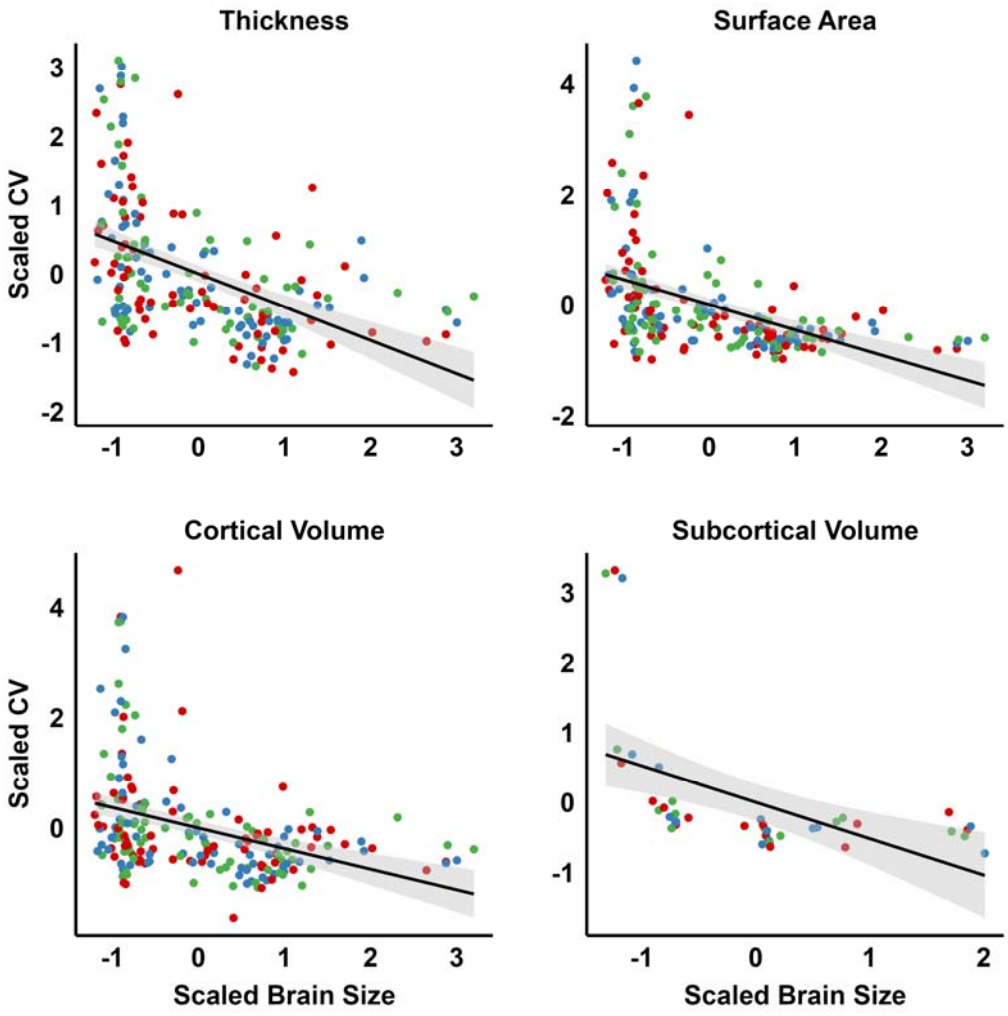

Fig. 9 The brain region size negatively correlated with CVs. The x-axis represents the scaled brain region size for the 34 (left and right) brain regions. The y-axis depicts the scaled CVs for the 34 (left and right) brain regions. The red color represents subject 1, the blue depicts subject 2, and the green represents subject 3.

4 Discussion

In this study, the within-subject stability of IDPs encompassing cortical thickness, surface area, and brain volume were examined. We first showed that the longitudinal stream of FreeSurfer generated more stable results compared to the cross-sectional stream. Furthermore, the stability of IDPs was quite high with most of the CVs and percentage change within 2% and 5%, respectively. Moreover, percentage changes in the cortical thickness strongly correlated with cortical volume while they correlated negatively with surface area. Lastly, the apparent head motion leads to an underestimation of cortical thickness and volume and an overestimation of surface area.

The longitudinal stream generates more reliable within-subject results, as suggeste by much smaller CVs (**Table 2**) and smaller percentage changes (**Fig. 1**) compared to the cross-sectional stream. The longitudinal stream was proposed in 2012 by the FreeSurfer team, and

since then it has been recommended for analyzing longitudinal datasets (Reuter et al., 2012). Specifically, the longitudinal stream creates and utilizes an unbiased within-subject template to generate a robust, inverse consistent registration, which boosts the stability and statistical power (Reuter et al., 2012; Vidal-Piñeiro et al., 2024). Indeed, our results are well in line with this argument. Accordingly, we also advocate the longitudinal stream should be used when analyzing longitudinal datasets.

4.1 The characteristics of IDPs

Cortical thickness is one of the IDPs of greatest interest in human brain research, given its role in defining normal cortical maturation (Bethlehem et al., 2022) and alterations observed in various neurological and mental disorders (Bethlehem et al., 2022; Frisoni, Fox, Jack, Scheltens, & Thompson, 2010; Lemaitre et al., 2012; Thompson et al., 2020). In our dataset, cortical thickness ranged from 1.50 to 4.03 mm (**Table S2**) which falls well within the known bounds of 1 and 4.5 mm (Fischl & Dale, 2000) indicating the validity of our dataset. Furthermore, we saw that the cortical thickness increases along the posterior-anterior axis (**Fig. S2A**), which is in concordance with the pattern documented in previous studies (Fischl & Dale, 2000; Hutton, De Vita, Ashburner, Deichmann, & Turner, 2008). Specifically, more detailed information has emerged based on the DK atlas, where we found that the insula, entorhinal cortex, and temporal pole are the thickest while the lingual gyrus, cuneus, and pericalcarine cortex are the thinnest (**Fig. S2B**). What's more, we observed that the thickest brain regions possess the largest standard deviations which agrees well with previous studies (Fischl & Dale, 2000; Hutton et al., 2008). Previous studies have also shown that the intersubjective standard deviations can be around 0.5 mm (Fischl & Dale, 2000; Hutton et al., 2008). Complement that, we found the within-subject standard deviations are much smaller, where most of them lie well below 0.05 mm with the thickest brain regions possessing the largest standard deviation of around 0.10 mm (**Table S2**). These results indicate that the cortical thickness measurement is very stable across a short time (about a year) in adults.

The surface area and brain volumes are the other two IDPs that can be constructed from the T1w images which can be used as a proxy index of the brain size (Genon et al., 2022). As expected, we saw large differences between subjects regarding brain sizes (**Table S3-S6**) where sub2 has the largest brain size followed by sub3 and sub1. This result highlights the importance of counterbalancing the brain size when comparing volume or surface area in a region between subjects. For example, it is common practice that ICV should be divided when comparing brain volumes between subjects instead of using absolute values (Bethlehem et al., 2022; Malone et al., 2015). Even though the brain size varies, based on the DK atlas, the biggest and smallest surface areas (**Fig. S4B**) and brain volumes (**Fig. S6B**) are the same within the three subjects. For example, regarding surface area, the superior parietal, rostral middle frontal, and superior frontal cortices are the largest while the entorhinal, transverse temporal, and frontal pole regions are the smallest. Moreover, the superior frontal and rostral middle frontal cortices are the largest for the cortical brain volume whereas the frontal pole and transverse temporal regions are the smallest. Additionally, for subcortical brain volume (**Fig. S9**), we show that the thalamus and putamen are the largest and the pallidum, amygdala, and accumbens area are the smallest. The DK atlas was developed based on curvature-based information such as the sulcal representations and the anatomic curvature (Desikan et al., 2006), therefore, the different size of the surface area and brain volume in different brain regions represent their own territories constrained by the curvature boundaries.

4.2 IDPs are stable across one year

We found that the IDPs including the cortical thickness, surface area, and brain volumes in the vast majority of the brain regions are stable, where CVs are well constrained at 2% and

the percentage change values are well within 5% over one year. CV and percentage change values have been used to evaluate the stability given that they are unitless and suitable for comparing variables with different sizes (Borga et al., 2020; Carbonell et al., 2022; M. Y. Wang et al., 2024; Y. Wang et al., 2021). CV is the division between standard deviation and average, where the smaller value denotes a much more stable measurement. In the same vein, percentage change is the division between the discrepancy and the average, where smaller values denote high stability and less variation. Generally, a measurement is considered reliable or stable when CVs are within 5 % or percentage changes are within 10% (Borga et al., 2020; Carbonell et al., 2022; M. Y. Wang et al., 2024; Y. Wang et al., 2021). For example, using CVs, it is found that the stability of brain metabolites such as N-acetyl-aspartate was reasonably high with CVs around 4% (M. Y. Wang et al., 2024). Therefore, the 2% of CVs in this study indicate that IDPs are fairly stable. In addition, the percentage change of 5% could encompass the annual 0.5 to 1 % decrease, for example in cortical brain volume, during adulthood (Lemaitre et al., 2012; Sele, Liem, Merillat, & Jancke, 2021; Storsve et al., 2014).

Although most of the brain regions are quite stable, several cortical brain regions did manifest larger fluctuations across all three IDPs, such as the temporal pole, frontal pole, pericalcarine, and entorhinal cortex. In addition, subcortical brain regions such as the accumbens area showed very high variations. The greater variation in IDPs in these regions is likely due to them being smaller and more difficult to parcellate (**Fig. 9**). Another speculation could be that these brain regions do vary that much, however, the underlying biological reason for it needs to be further investigated. Future studies are warranted to explore this issue. Finally, only subject 2 manifested high variability in the cingulate cortex especially the PCC compared to the other two participants indicating that individual differences can influence the temporal stability of IDPs.

4.3 Cortical thickness changes together with cortical volume but not with surface area

We found that the overall association within each phenotype was quite similar (**Fig. 6A-C**) with an average strength of around 0.25. On the contrary, the relationships between each phenotype are quite divergent (**Fig. 6D-F**). Specifically, the percentage changes in cortical thickness and volume manifested a strong positive correlation while both of them illustrated a weak correlation with the percentage change of surface area. More importantly, the percentage changes in the cortical thickness showed a negative correlation with that of the surface area. These short-timescale results corroborate well with the long-timescale normal aging study (Storsve et al., 2014). Collectively, these results reinforce that cortical thickness and surface area play distinct roles in brain anatomy and aging (Lemaitre et al., 2012; Storsve et al., 2014; Vijayakumar et al., 2016), which is sensible since they have distinct genetic roots (Panizzon et al., 2009).

4.4 The time-of-day and daylight-hour effects

We found no time-of-day effect (meta-analysis results) on average cortical thickness, total surface area, and total brain volumes (**Fig. 7**). Previous studies, however, have reported significantly thinner cortical thickness (Trefler et al., 2016) and smaller brain volume (Karch et al., 2019; Nakamura et al., 2015; Trefler et al., 2016) in the afternoon compared to the morning. In this study, IDPs did show smaller values in the afternoon sessions but were not significantly different from the morning sessions. The discrepancy between our results and others could result from the following reasons. First, this study is a within-subject design while two of the other studies were between-subject design (Nakamura et al., 2015; Trefler et al., 2016), from which the intersubjective variation could obstruct the reported time-of-day effect. Second, this study has recorded at least 10 sessions and up to 23 sessions for each subject in the morning or afternoon sessions whereas the other studies either had one data

point (Nakamura et al., 2015) or two data points for morning and afternoon sessions in their primary and secondary datasets (Trefler et al., 2016). Fourth, although one is a within-subject design (Karch et al., 2019), the longitudinal stream, which will provide more robust results as also evidenced by this study and others (Reuter et al., 2012), was not implemented.

Although no time-of-day effects were uncovered in our study, we could not rule out (equivalent test results) that there is no true time-of-day effect on average cortical thickness and total subcortical brain volume given the effect size of 0.5 (**Fig. 7**). The results were largely driven by subject 1 on the average cortical thickness and by subject 2 on the total subcortical brain volume manifesting the inter-individual characteristics, from which studies with more subjects with within-subject design are needed to reconcile this effect. But before that, we recommend that when estimating the abovementioned two IDPs, the time-of-day effect should be considered since their effect sizes were not too trivial to be ignored. However, the time-of-day effect on the total cortical brain volume and total surface area was subtle with which the factor could be ignored.

Similarly, we found no daylight-hour effect (meta-analysis) on average cortical thickness, and total brain volumes but not total surface area. Previous studies have focused on the seasonal effect (Zhang et al., 2023) on functional brain organization and stated that daylight could reconfigure the resting state brain networks (M. Y. Wang et al., 2023b). However, to the best of our knowledge, this study could be the first study directly investigating the daylight effect on T1w-derived phenotypes. Although there is a daylight-hour effect on the total surface area, the effect size is too small to be considered significant. On the other hand, the non-effect on the total subcortical brain volume could not be ruled out. However, this could partially be due to the instability of the accumbens area, which also leads to similar results of the time-of-day effect. Taken together, we could suggest that the daylight hours could be left out when estimating the IDPs.

Regarding the equivalent test to the time-of-day and daylight-hour effects, to be noticed, deciding whether the effect size is too trivial is heavily dependent on the predefined effect size (Lakens, 2017; Lakens et al., 2018). In this study, an effect size of 0.5 was used, one could argue that the effect size could be set at 0.3 or 0.8 depending on the objectives of one's studies (Lakens, 2017; Lakens et al., 2018).

4.5 Head motion underestimates thickness and volume whereas it overestimates surface area

Head motion can be indicated by the CJV values, with higher CJV values denoting apparent head motion, which could deteriorate the SNR and CNR, and blur the image (Ganzetti et al., 2016). After excluding the two sessions with excessive head motion in subject 3, the stability of all the T1w-derived phenotypes has been significantly improved evidenced by smaller CVs (**Table 8**) and percentage changes (**Fig. 8**). However, the pattern is different. On one hand, the cortical thickness and cortical volume estimation were increased indicating the underestimation induced by head motion, which is in concordance with the previous study (Reuter et al., 2015). On the other hand, the surface area measurement is decreased indicating that head motion causes tsurface area to be underestimated. This result indicates that the head motion evaluation should be controlled especially when investigating participants who move a lot such as autistic children or Parkinson's patients (Reuter et al., 2015).

4.6 Limitations

Several limitations should be articulated before any conclusions. First, lacking female subjects hampers the generalization of our results. It is known that major events such as pregnancy (Hoekzema et al., 2017) and hormone levels can alter brain structure (Rizor et al.,

2024). Second, although using the same MRI scanner and the same data processing stream can alleviate the interference from heterogeneous ones, it could impede the application to other datasets that are collected on other MRI scanners or data processing streams. Third, the timing of data collection was not fixed for each subject, for example, sub1 was not scanned at 10 AM on Mondays, instead, each subject was scanned based on the availability of the scanning time and their available time. Lastly, we acknowledge that the results are a mixture of the measurement (T1w) and the measure (MRI machine). Although the results indicate the IDPs are stable, it could be informative if the two sources could be separated, for example, using a phantom to evaluate the stability of the MRI machine and deduct from the current results which could lead to the measurement (T1w) stability.

5. Conclusion

In summary, the stability of T1w-derived phenotypes across one year during adulthood is fairly high with CVs within 2% while percentage changes within 5%. However, several brain regions including the temporal pole, frontal pole, pericalcarine, entorhinal cortex, and accumbens area did manifest larger fluctuations. Moreover, head motion leads to the underestimation of the cortical thickness and volume while overestimation of the surface area. Furthermore, daylight length might be useful when evaluating the total subcortical brain volume, but less relevant for other regions' volume estimates. Lastly, time of day might be a confound when evaluating cortical thickness and subcortical brain volumes.

Data and Code Availability

Data and code used in this manuscript can be found here on GitHub https://github.com/MengYunWang/BBSC/tree/main/fMRI/T1_analysis.

Author Contributions

Meng-Yun Wang: Conceptualization, Data collection & curation, Formal analysis, Investigation, Methodology, Project administration, Visualization, Writing—original draft, and Writing—review & editing. Max Korbmacher: Conceptualization, Data collection, and Writing—review & editing. Rune Eikeland: Conceptualization, Data collection, Writing—review & editing. Stener Nerland: Methodology, Writing—review & editing. Didac Vidal-Pineiro: Methodology, Writing—review & editing. Karsten Specht: Conceptualization, Writing—review & editing, Funding acquisition.

Funding

This study was financed by the Research Council of Norway (Project number: 276044: When default is not default: Solutions to the replication crisis and beyond).

Ethics Statement

All participants have understood and signed written informed consent. The project was conducted according to the principles expressed in the Declaration of Helsinki. Ethics approval was granted by the Regional Committees for Medical and Health Research Ethics (REK-vest).

Declaration of Competing Interests

No declared conflicts of interest.

Acknowledgments

We appreciate the technical support and data collection support from our radiologists (Christel Jansen, Eva Øksnes, Roger Barndon, Trond Øvreaas, Tor Fjørtoft, and Turid Randa) at the Haukeland University Hospital.

References

Alexander-Bloch, A., Clasen, L., Stockman, M., Ronan, L., Lalonde, F., Giedd, J., & Raznahan, A. (2016). Subtle In-Scanner Motion Biases Automated Measurement of Brain Anatomy From In Vivo MRI. *Human Brain Mapping, 37*(7), 2385-2397. doi:10.1002/hbm.23180

Bethlehem, R. A. I., Seidlitz, J., White, S. R., Vogel, J. W., Anderson, K. M., Adamson, C., . . . Alexander-Bloch, A. F. (2022). Brain charts for the human lifespan. *Nature, 604*(7906), 525-533. doi:10.1038/s41586-022-04554-y

Borga, M., Ahlgren, A., Romu, T., Widholm, P., Leinhard, O. D., & West, J. (2020). Reproducibility and repeatability of MRI-based body composition analysis. *Magnetic Resonance in Medicine, 84*(6), 3146-3156. doi:10.1002/mrm.28360

Brandmaier, A. M., Wenger, E., Bodammer, N. C., Kühn, S., Raz, N., & Lindenberger, U. (2018). Assessing reliability in neuroimaging research through intra-class effect decomposition (ICED). *Elife, 7*. doi:10.7554/eLife.35718

Carbonell, G., Kennedy, P., Bane, O., Kirmani, A., El Homsi, M., Stocker, D., . . . Taouli, B. (2022). Precision of MRI radiomics features in the liver and hepatocellular carcinoma. *European Radiology, 32*(3), 2030-2040. doi:10.1007/s00330-021-08282-1

Chen, C. H., Gutierrez, E. D., Thompson, W., Panizzon, M. S., Jernigan, T. L., Eyler, L. T., . . . Dale, A. M. (2012). Hierarchical genetic organization of human cortical surface area. *Science, 335*(6076), 1634-1636. doi:10.1126/science.1215330

Dale, A. M., Fischl, B., & Sereno, M. I. (1999). Cortical surface-based analysis. I. Segmentation and surface reconstruction. *Neuroimage, 9*(2), 179-194. doi:10.1006/nimg.1998.0395

Desikan, R. S., Segonne, F., Fischl, B., Quinn, B. T., Dickerson, B. C., Blacker, D., . . . Killiany, R. J. (2006). An automated labeling system for subdividing the human cerebral cortex on MRI scans into gyral based regions of interest. *Neuroimage, 31*(3), 968-980. doi:10.1016/j.neuroimage.2006.01.021

Di, X., Woelfer, M., Kühn, S., Zhang, Z. G., & Biswal, B. B. (2022). Estimations of the weather effects on brain functions using functional MRI: A cautionary note. *Human Brain Mapping, 43*(11), 3346-3356. doi:10.1002/hbm.25576

Ducharme, S., Albaugh, M. D., Nguyen, T. V., Hudziak, J. J., Mateos-Perez, J. M., Labbe, A., . . . Brain Development Cooperative, G. (2016). Trajectories of cortical thickness maturation in normal brain development--The importance of quality control procedures. *Neuroimage, 125*, 267-279. doi:10.1016/j.neuroimage.2015.10.010

Elliott, L. T., Sharp, K., Alfaro-Almagro, F., Shi, S., Miller, K. L., Douaud, G., . . . Smith, S. M. (2018). Genome-wide association studies of brain imaging phenotypes in UK Biobank. *Nature, 562*(7726), 210-216. doi:10.1038/s41586-018-0571-7

Elliott, M. L., Knodt, A. R., Ireland, D., Morris, M. L., Poulton, R., Ramrakha, S., . . . Hariri, A. R. (2020). What Is the Test-Retest Reliability of Common Task-Functional MRI Measures? New Empirical Evidence and a Meta-Analysis. *Psychological Science, 31*(7), 792-806. doi:10.1177/0956797620916786

Esteban, O., Birman, D., Schaer, M., Koyejo, O. O., Poldrack, R. A., & Gorgolewski, K. J. (2017). MRIQC: Advancing the automatic prediction of image quality in MRI from unseen sites. *Plos One, 12*(9), e0184661. doi:10.1371/journal.pone.0184661

Fischl, B., & Dale, A. M. (2000). Measuring the thickness of the human cerebral cortex from magnetic resonance images. *Proc Natl Acad Sci U S A, 97*(20), 11050-11055. doi:10.1073/pnas.200033797

Fischl, B., Sereno, M. I., & Dale, A. M. (1999). Cortical surface-based analysis. II: Inflation, flattening, and a surface-based coordinate system. *Neuroimage, 9*(2), 195-207. doi:10.1006/nimg.1998.0396

Frisoni, G. B., Fox, N. C., Jack, C. R., Jr., Scheltens, P., & Thompson, P. M. (2010). The clinical use of structural MRI in Alzheimer disease. *Nature Reviews Neurology, 6*(2), 67-77. doi:10.1038/nrneurol.2009.215

Ganzetti, M., Wenderoth, N., & Mantini, D. (2016). Intensity Inhomogeneity Correction of Structural MR Images: A Data-Driven Approach to Define Input Algorithm Parameters. *Frontiers in Neuroinformatics, 10*, 10. doi:10.3389/fninf.2016.00010

Genon, S., Eickhoff, S. B., & Kharabian, S. (2022). Linking interindividual variability in brain structure to behaviour. *Nature Reviews Neuroscience, 23*(5), 307-318. doi:10.1038/s41583-022-00584-7

Grasby, K. L., Jahanshad, N., Painter, J. N., Colodro-Conde, L., Bralten, J., Hibar, D. P., . . . Group, E. N. G. t. M.-A. C.-G. W. (2020). The genetic architecture of the human cerebral cortex. *Science, 367*(6484), eaay6690. doi:10.1126/science.aay6690

Gronenschild, E. H., Habets, P., Jacobs, H. I., Mengelers, R., Rozendaal, N., van Os, J., & Marcelis, M. (2012). The effects of FreeSurfer version, workstation type, and Macintosh operating system version on anatomical volume and cortical thickness measurements. *Plos One, 7*(6), e38234. doi:10.1371/journal.pone.0038234

Han, X., Jovicich, J., Salat, D., van der Kouwe, A., Quinn, B., Czanner, S., . . . Fischl, B. (2006). Reliability of MRI-derived measurements of human cerebral cortical thickness: the effects of field strength, scanner upgrade and manufacturer. *Neuroimage, 32*(1), 180-194. doi:10.1016/j.neuroimage.2006.02.051

Hoekzema, E., Barba-Müller, E., Pozzobon, C., Picado, M., Lucco, F., García-García, D., . . . Vilarroya, O. (2017). Pregnancy leads to long-lasting changes in human brain structure. *Nature Neuroscience, 20*(2), 287-296. doi:10.1038/nn.4458

Holz, N. E., Zabihi, M., Kia, S. M., Monninger, M., Aggensteiner, P. M., Siehl, S., . . . Marquand, A. F. (2023). A stable and replicable neural signature of lifespan adversity in the adult brain. *Nature Neuroscience, 26*(9), 1603-1612. doi:10.1038/s41593-023-01410-8

Hutton, C., De Vita, E., Ashburner, J., Deichmann, R., & Turner, R. (2008). Voxel-based cortical thickness measurements in MRI. *Neuroimage, 40*(4), 1701-1710. doi:10.1016/j.neuroimage.2008.01.027

Iscan, Z., Jin, T. B., Kendrick, A., Szeglin, B., Lu, H., Trivedi, M., . . . DeLorenzo, C. (2015). Test-retest reliability of freesurfer measurements within and between sites: Effects of visual approval process. *Human Brain Mapping, 36*(9), 3472-3485. doi:10.1002/hbm.22856

Karch, J. D., Filevich, E., Wenger, E., Lisofsky, N., Becker, M., Butler, O., . . . Kuhn, S. (2019). Identifying predictors of within-person variance in MRI-based brain volume estimates. *Neuroimage, 200*, 575-589. doi:10.1016/j.neuroimage.2019.05.030

Korbmacher, M., Wang, M. Y., Eikeland, R., Buchert, R., Andreassen, O. A., Espeseth, T., . . . Specht, K. (2023). Considerations on brain age predictions from repeatedly sampled data across time. *Brain and Behavior, 13*(10). doi:10.1002/brb3.3219

Lakens, D. (2017). Equivalence Tests: A Practical Primer for t Tests, Correlations, and Meta-Analyses *Social Psychological and Personality Science, 8*(4), 355-362. doi:10.1177/1948550617697177

Lakens, D., Scheel, A. M., & Isager, P. M. (2018). Equivalence Testing for Psychological Research: A Tutorial. *Advances in Methods and Practices in Psychological Science, 1*(2), 259-269. doi:10.1177/2515245918770963

Lemaitre, H., Goldman, A. L., Sambataro, F., Verchinski, B. A., Meyer-Lindenberg, A., Weinberger, D. R., & Mattay, V. S. (2012). Normal age-related brain morphometric changes: nonuniformity across cortical thickness, surface area and gray matter volume?

Neurobiology of Aging, *33*(3), 617 e611-619. doi:10.1016/j.neurobiolaging.2010.07.013

Lerch, J. P., van der Kouwe, A. J., Raznahan, A., Paus, T., Johansen-Berg, H., Miller, K. L., . . . Sotiropoulos, S. N. (2017). Studying neuroanatomy using MRI. *Nature Neuroscience*, *20*(3), 314-326. doi:10.1038/nn.4501

Malone, I. B., Leung, K. K., Clegg, S., Barnes, J., Whitwell, J. L., Ashburner, J., . . . Ridgway, G. R. (2015). Accurate automatic estimation of total intracranial volume: A nuisance variable with less nuisance. *Neuroimage*, *104*, 366-372. doi:10.1016/j.neuroimage.2014.09.034

Mowinckel, A. M., & Vidal-Piñeiro, D. (2020). Visualization of Brain Statistics With R Packages ggseg and ggseg3d. *Advances in Methods and Practices in Psychological Science*, *3*(4), 466-483. doi:10.1177/2515245920928009

Nakamura, K., Brown, R. A., Narayanan, S., Collins, D. L., Arnold, D. L., & Alzheimer's Disease Neuroimaging, I. (2015). Diurnal fluctuations in brain volume: Statistical analyses of MRI from large populations. *Neuroimage*, *118*, 126-132. doi:10.1016/j.neuroimage.2015.05.077

Noble, S., Scheinost, D., & Constable, R. T. (2021). A guide to the measurement and interpretation of fMRI test-retest reliability. *Current Opinion in Behavioral Sciences*, *40*, 27-32. doi:10.1016/j.cobeha.2020.12.012

Noble, S., Spann, M. N., Tokoglu, F., Shen, X. L., Constable, R. T., & Scheinost, D. (2017). Influences on the Test-Retest Reliability of Functional Connectivity MRI and its Relationship with Behavioral Utility. *Cerebral Cortex*, *27*(11), 5415-5429. doi:10.1093/cercor/bhx230

Orban, C., Kong, R., Li, J. W., Chee, M. W. L., & Yeo, B. T. T. (2020). Time of day is associated with paradoxical reductions in global signal fluctuation and functional connectivity. *Plos Biology*, *18*(2). doi:10.1371/journal.pbio.3000602

Panizzon, M. S., Fennema-Notestine, C., Eyler, L. T., Jernigan, T. L., Prom-Wormley, E., Neale, M., . . . Kremen, W. S. (2009). Distinct genetic influences on cortical surface area and cortical thickness. *Cerebral Cortex*, *19*(11), 2728-2735. doi:10.1093/cercor/bhp026

Parsons, S., Brandmaier, A. M., Lindenberger, U., & Kievit, R. (2024). Longitudinal stability of cortical grey matter measures varies across brain regions, imaging metrics, and testing sites in the ABCD study. *Imaging Neuroscience*, *2*, 1-22. doi:10.1162/imag_a_00086

Reuter, M., Rosas, H. D., & Fischl, B. (2010). Highly accurate inverse consistent registration: a robust approach. *Neuroimage*, *53*(4), 1181-1196. doi:10.1016/j.neuroimage.2010.07.020

Reuter, M., Schmansky, N. J., Rosas, H. D., & Fischl, B. (2012). Within-subject template estimation for unbiased longitudinal image analysis. *Neuroimage*, *61*(4), 1402-1418. doi:10.1016/j.neuroimage.2012.02.084

Reuter, M., Tisdall, M. D., Qureshi, A., Buckner, R. L., van der Kouwe, A. J. W., & Fischl, B. (2015). Head motion during MRI acquisition reduces gray matter volume and thickness estimates. *Neuroimage*, *107*, 107-115. doi:10.1016/j.neuroimage.2014.12.006

Rizor, E. J., Babenko, V., Dundon, N. M., Beverly-Aylwin, R., Stump, A., Hayes, M., . . . Grafton, S. T. (2024). Menstrual cycle-driven hormone concentrations co-fluctuate with white and gray matter architecture changes across the whole brain. *Human Brain Mapping*, *45*(11). doi:10.1002/hbm.26785

Sele, S., Liem, F., Merillat, S., & Jancke, L. (2021). Age-related decline in the brain: a longitudinal study on inter-individual variability of cortical thickness, area, volume, and cognition. *Neuroimage, 240*, 118370. doi:10.1016/j.neuroimage.2021.118370

Sowell, E. R., Peterson, B. S., Thompson, P. M., Welcome, S. E., Henkenius, A. L., & Toga, A. W. (2003). Mapping cortical change across the human life span. *Nature Neuroscience, 6*(3), 309-315. doi:10.1038/nn1008

Sowell, E. R., Thompson, P. M., Leonard, C. M., Welcome, S. E., Kan, E., & Toga, A. W. (2004). Longitudinal mapping of cortical thickness and brain growth in normal children. *Journal of Neuroscience, 24*(38), 8223-8231. doi:10.1523/JNEUROSCI.1798-04.2004

Storsve, A. B., Fjell, A. M., Tamnes, C. K., Westlye, L. T., Overbye, K., Aasland, H. W., & Walhovd, K. B. (2014). Differential longitudinal changes in cortical thickness, surface area and volume across the adult life span: regions of accelerating and decelerating change. *Journal of Neuroscience, 34*(25), 8488-8498. doi:10.1523/JNEUROSCI.0391-14.2014

Thompson, P. M., Jahanshad, N., Ching, C. R. K., Salminen, L. E., Thomopoulos, S. I., Bright, J., . . . Consortium, E. (2020). ENIGMA and global neuroscience: A decade of large-scale studies of the brain in health and disease across more than 40 countries. *Transl Psychiatry, 10*(1), 100. doi:10.1038/s41398-020-0705-1

Trefler, A., Sadeghi, N., Thomas, A. G., Pierpaoli, C., Baker, C. I., & Thomas, C. (2016). Impact of time-of-day on brain morphometric measures derived from T1-weighted magnetic resonance imaging. *Neuroimage, 133*, 41-52. doi:10.1016/j.neuroimage.2016.02.034

Vidal-Piñeiro, D., Sørensen, Ø., Strømstad, M., Amlien, I. K., Anderson, M., Baaré, W. F. C., . . . Fjell, A. M. (2024). Reliability of structural brain change in cognitively healthy adult samples. *bioRxiv*, 2024.2006.2003.592804. doi:10.1101/2024.06.03.592804

Vidal-Pineiro, D., Wang, Y. P., Krogsrud, S. K., Amlien, I. K., Baaré, W. F., Bartres-Faz, D., . . . Fjell, A. (2021). Individual variations in 'brain age' relate to early-life factors more than to longitudinal brain change. *Elife, 10*. doi:10.7554/eLife.69995

Viechtbauer, W. (2010). Conducting Meta-Analyses in R with the metafor Package. *Journal of Statistical Software, 36*(3), 1-48. doi:DOI 10.18637/jss.v036.i03

Vijayakumar, N., Allen, N. B., Youssef, G., Dennison, M., Yucel, M., Simmons, J. G., & Whittle, S. (2016). Brain development during adolescence: A mixed-longitudinal investigation of cortical thickness, surface area, and volume. *Human Brain Mapping, 37*(6), 2027-2038. doi:10.1002/hbm.23154

Wang, M. Y., Korbmacher, M., Eikeland, R., Craven, A. R., & Specht, K. (2024). The intra-individual reliability of 1H-MRS measurement in the anterior cingulate cortex across 1 year. *Human Brain Mapping, 45*(1), e26531. doi:10.1002/hbm.26531

Wang, M. Y., Korbmacher, M., Eikeland, R., & Specht, K. (2022). Deep brain imaging of three participants across 1 year: The Bergen breakfast scanning club project. *Frontiers in Human Neuroscience, 16*, 1021503. doi:10.3389/fnhum.2022.1021503

Wang, M. Y., Korbmacher, M., Eikeland, R., & Specht, K. (2023a). The Bergen Breakfast Scanning Club dataset: a deep brain imaging dataset. *bioRxiv*, 2023.2005.2030.542072. doi:10.1101/2023.05.30.542072

Wang, M. Y., Korbmacher, M., Eikeland, R., & Specht, K. (2023b). *The long night effect on the brain functional organization*. Paper presented at the The Organization for Human Brain Mapping 2023, Vancouver, Canada.

Wang, Y., Tadimalla, S., Rai, R., Goodwin, J., Foster, S., Liney, G., . . . Haworth, A. (2021). Quantitative MRI: Defining repeatability, reproducibility and accuracy for prostate

cancer imaging biomarker development. *Magnetic Resonance Imaging, 77*, 169-179. doi:10.1016/j.mri.2020.12.018

Wickham, H. (2009). ggplot2: Elegant Graphics for Data Analysis. *Ggplot2: Elegant Graphics for Data Analysis*, 1-212. doi:10.1007/978-0-387-98141-3

Wu, J., Li, J., Eickhoff, S. B., Scheinost, D., & Genon, S. (2023). The challenges and prospects of brain-based prediction of behaviour. *Nature Human Behaviour, 7*(8), 1255-1264. doi:10.1038/s41562-023-01670-1

Yeo, B. T., Krienen, F. M., Sepulcre, J., Sabuncu, M. R., Lashkari, D., Hollinshead, M., . . . Buckner, R. L. (2011). The organization of the human cerebral cortex estimated by intrinsic functional connectivity. *Journal of Neurophysiology, 106*(3), 1125-1165. doi:10.1152/jn.00338.2011

Zhang, R., Shokri-Kojori, E., & Volkow, N. D. (2023). Seasonal effect-an overlooked factor in neuroimaging research. *Translational Psychiatry, 13*(1). doi:10.1038/s41398-023-02530-2

Zuo, X. N., Xu, T., & Milham, M. P. (2019). Harnessing reliability for neuroscience research. *Nature Human Behaviour, 3*(8), 768-771. doi:10.1038/s41562-019-0655-x

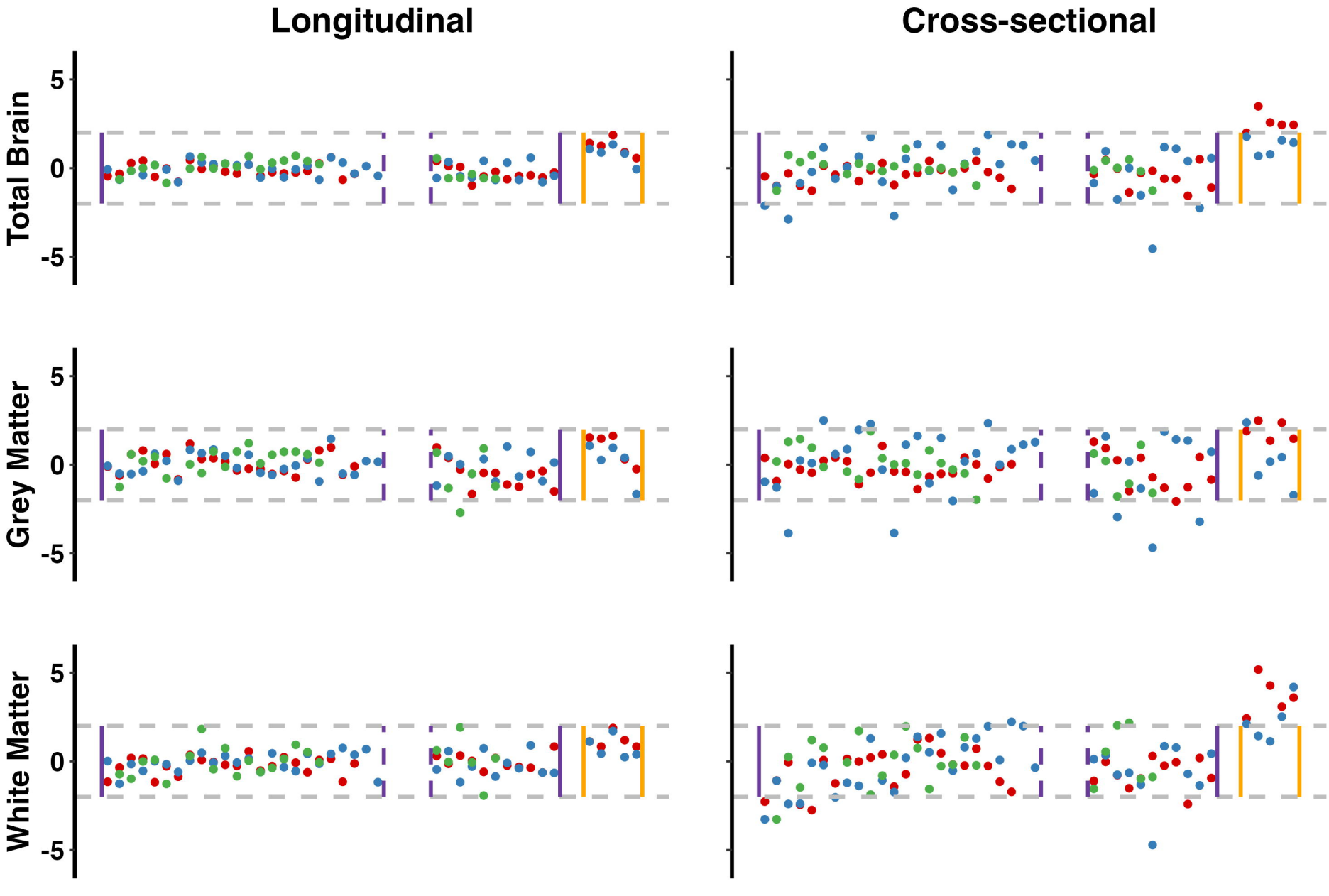
Longitudinal
Cross-sectional
Total Brain
Grey Matter
White Matter
5
0
-5

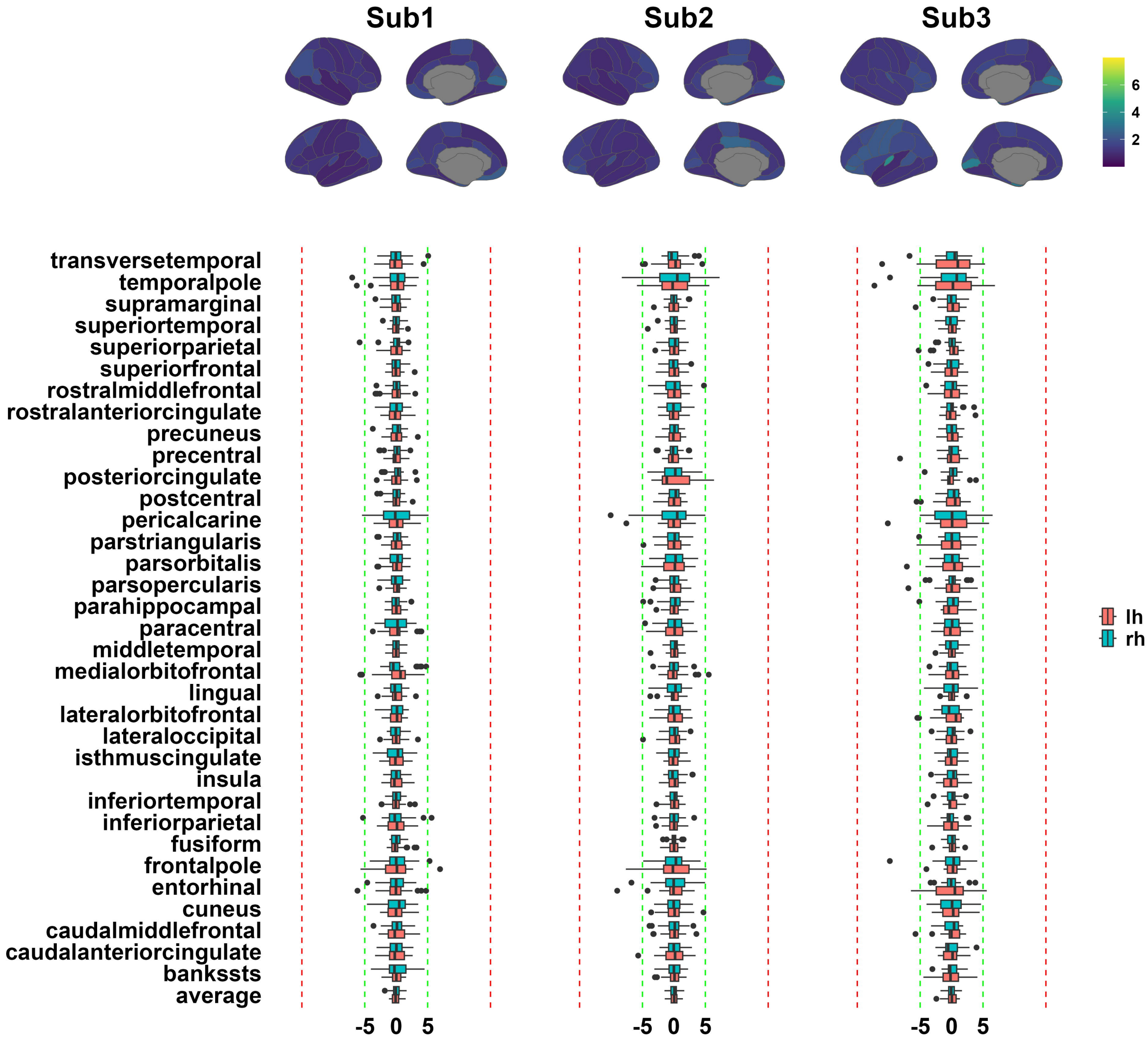
Sub1
Sub2
Sub3
6
4
2
transversetemporal
temporalpole
supramarginal
superiortemporal
superiorparietal
superiorfrontal
rostralmiddlefrontal
rostralanteriorcingulate
precuneus
precentral
posteriorcingulate
postcentral
pericalcarine
parstriangularis
parsorbitalis
parsopercularis
parahippocampal
paracentral
middletemporal
medialorbitofrontal
lingual
lateralorbitofrontal
lateraloccipital
isthmuscingulate
insula
inferiortemporal
inferiorparietal
fusiform
frontalpole
entorhinal
cuneus
caudalmiddlefrontal
caudalanteriorcingulate
bankssts
average
-5 0 5
-5 0 5
-5 0 5
lh
rh

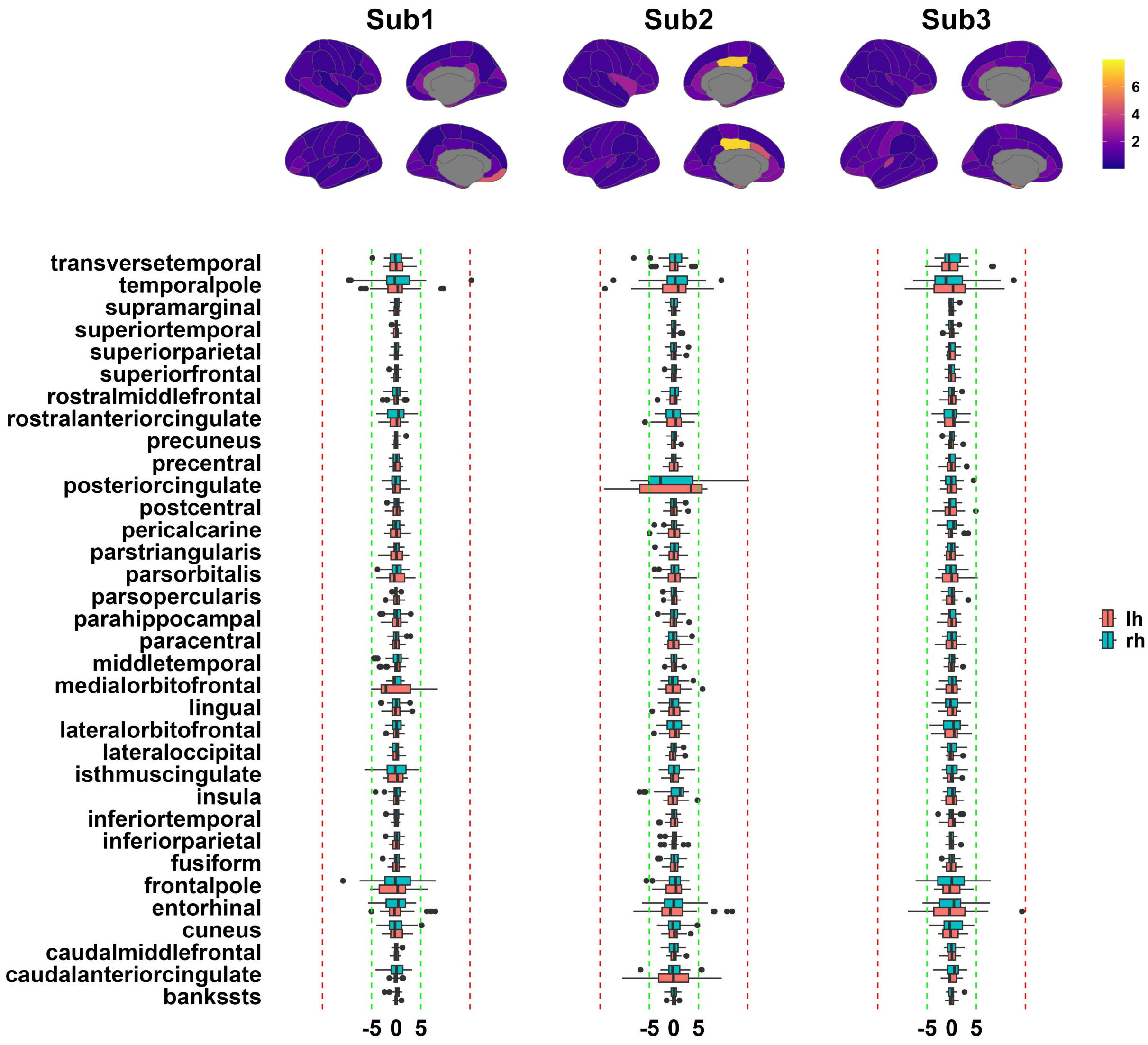
Sub1
Sub2
Sub3
6
4
2
transversetemporal
temporalpole
supramarginal
superiortemporal
superiorparietal
superiorfrontal
rostralmiddlefrontal
rostralanteriorcingulate
precuneus
precentral
posteriorcingulate
postcentral
pericalcarine
parstriangularis
parsorbitalis
parsopercularis
parahippocampal
paracentral
middletemporal
medialorbitofrontal
lingual
lateralorbitofrontal
lateraloccipital
isthmuscingulate
insula
inferiortemporal
inferiorparietal
fusiform
frontalpole
entorhinal
cuneus
caudalmiddlefrontal
caudalanteriorcingulate
bankssts
-5 0 5
-5 0 5
-5 0 5
lh
rh

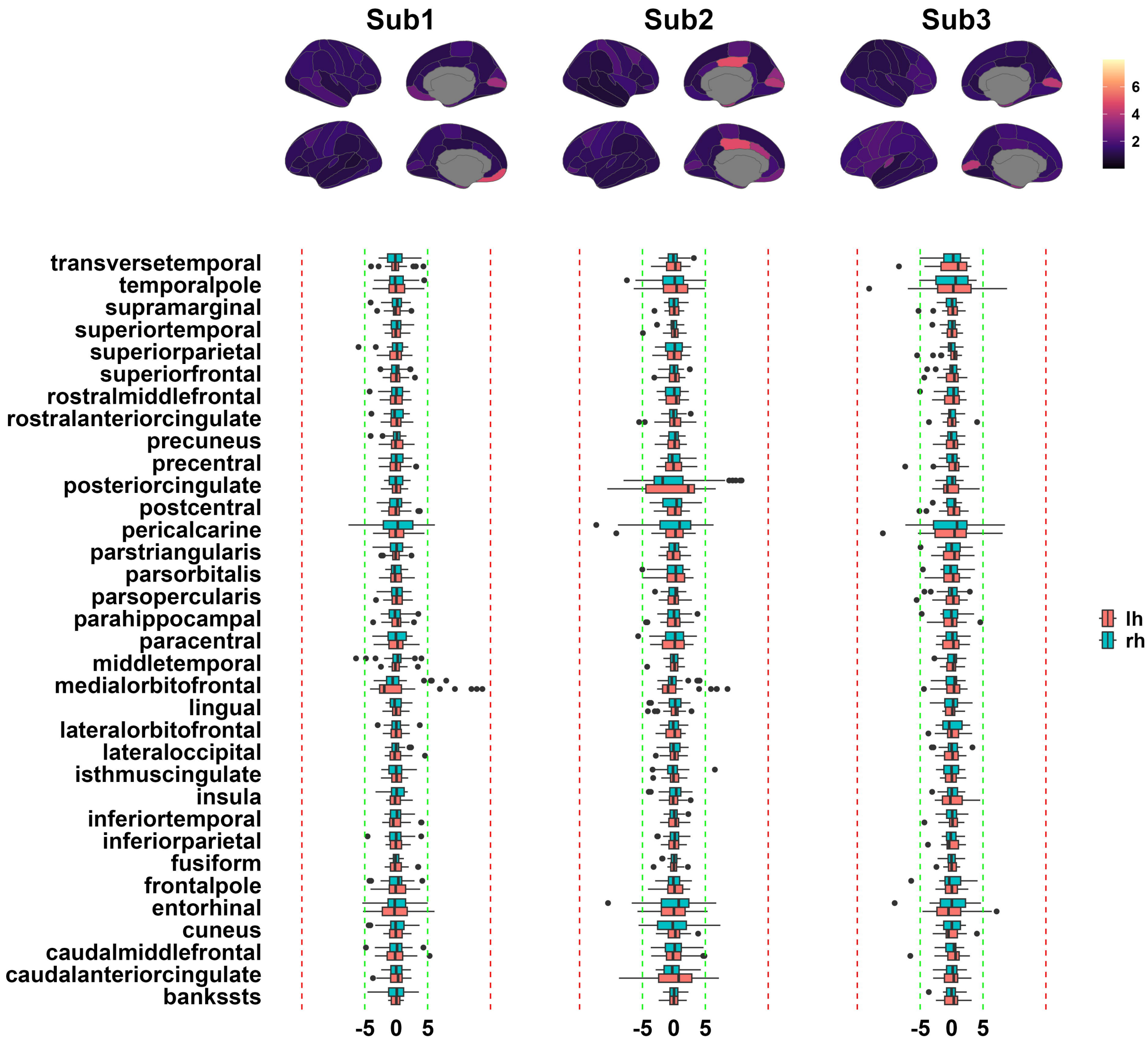
Sub1
Sub2
Sub3
6
4
2
transversetemporal
temporalpole
supramarginal
superiortemporal
superiorparietal
superiorfrontal
rostralmiddlefrontal
rostralanteriorcingulate
precuneus
precentral
posteriorcingulate
postcentral
pericalcarine
parstriangularis
parsorbitalis
parsopercularis
parahippocampal
paracentral
middletemporal
medialorbitofrontal
lingual
lateralorbitofrontal
lateraloccipital
isthmuscingulate
insula
inferiortemporal
inferiorparietal
fusiform
frontalpole
entorhinal
cuneus
caudalmiddlefrontal
caudalanteriorcingulate
bankssts
-5 0 5
-5 0 5
-5 0 5
lh
rh

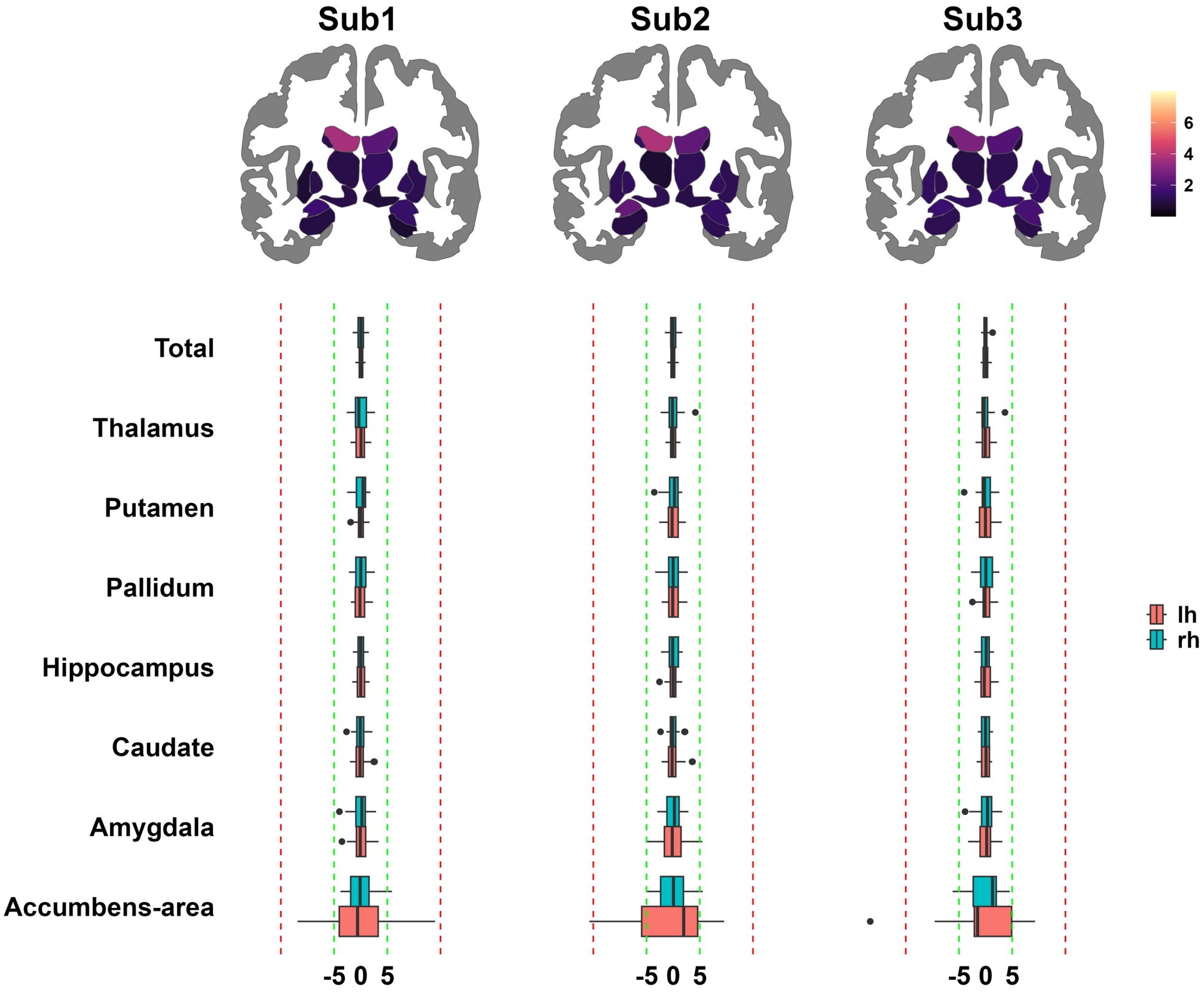
Sub1
Sub2
Sub3
6
4
2
Total
Thalamus
Putamen
Pallidum
Hippocampus
Caudate
Amygdala
Accumbens-area
lh
rh
-5 0 5
-5 0 5
-5 0 5

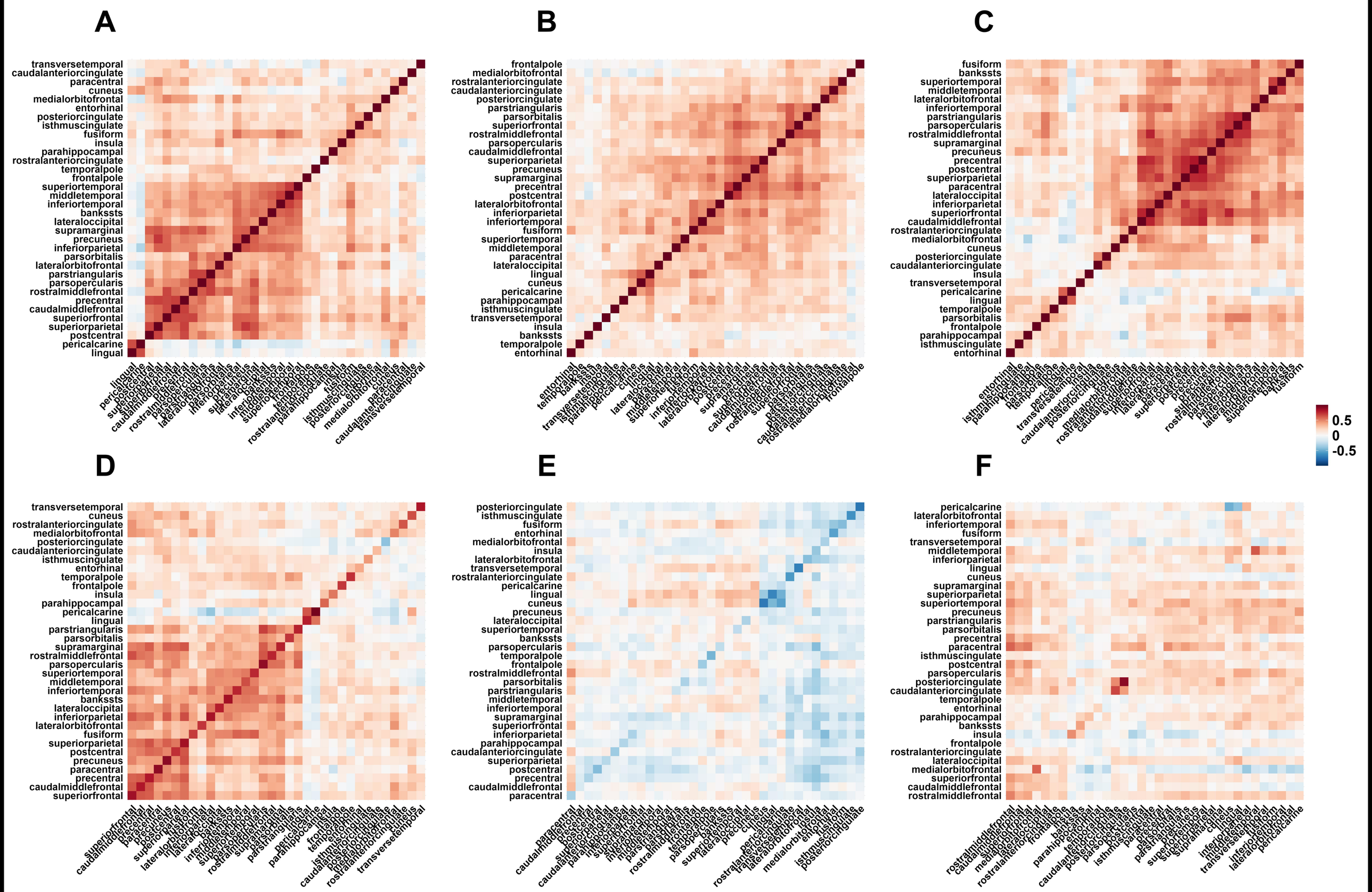
A
transversetemporal
caudalanteriorcingulate
paracentral
cuneus
medialorbitofrontal
entorhinal
posteriorcingulate
isthmuscingulate
fusiform
insula
parahippocampal
rostralanteriorcingulate
temporalpole
frontalpole
superiortemporal
middletemporal
inferiortemporal
bankssts
lateraloccipital
supramarginal
precuneus
inferiorparietal
parsorbitalis
lateralorbitofrontal
parstriangularis
parsopercularis
rostralmiddlefrontal
precentral
caudalmiddlefrontal
superiorfrontal
superiorparietal
postcentral
pericalcarine
lingual
B
frontalpole
medialorbitofrontal
rostralanteriorcingulate
caudalanteriorcingulate
posteriorcingulate
parstriangularis
parsorbitalis
superiorfrontal
rostralmiddlefrontal
parsopercularis
caudalmiddlefrontal
superiorparietal
precuneus
supramarginal
precentral
postcentral
lateralorbitofrontal
inferiorparietal
inferiortemporal
fusiform
superiortemporal
middletemporal
paracentral
lateraloccipital
lingual
cuneus
pericalcarine
parahippocampal
isthmuscingulate
transversetemporal
insula
bankssts
temporalpole
entorhinal
C
fusiform
bankssts
superiortemporal
middletemporal
lateralorbitofrontal
inferiortemporal
parstriangularis
parsopercularis
rostralmiddlefrontal
supramarginal
precuneus
precentral
postcentral
superiorparietal
paracentral
lateraloccipital
inferiorparietal
superiorfrontal
caudalmiddlefrontal
rostralanteriorcingulate
medialorbitofrontal
cuneus
posteriorcingulate
caudalanteriorcingulate
insula
transversetemporal
pericalcarine
lingual
temporalpole
parsorbitalis
frontalpole
parahippocampal
isthmuscingulate
entorhinal
0.5
0
-0.5
D
transversetemporal
cuneus
rostralanteriorcingulate
medialorbitofrontal
posteriorcingulate
caudalanteriorcingulate
isthmuscingulate
entorhinal
temporalpole
frontalpole
insula
parahippocampal
pericalcarine
lingual
parstriangularis
parsorbitalis
supramarginal
rostralmiddlefrontal
parsopercularis
superiortemporal
middletemporal
inferiortemporal
bankssts
lateraloccipital
inferiorparietal
lateralorbitofrontal
fusiform
superiorparietal
postcentral
precuneus
paracentral
precentral
caudalmiddlefrontal
superiorfrontal
E
posteriorcingulate
isthmuscingulate
fusiform
entorhinal
medialorbitofrontal
insula
lateralorbitofrontal
transversetemporal
rostralanteriorcingulate
pericalcarine
lingual
cuneus
precuneus
lateraloccipital
superiortemporal
bankssts
parsopercularis
temporalpole
frontalpole
rostralmiddlefrontal
parsorbitalis
parstriangularis
middletemporal
inferiortemporal
supramarginal
superiorfrontal
inferiorparietal
parahippocampal
caudalanteriorcingulate
superiorparietal
postcentral
precentral
caudalmiddlefrontal
paracentral
F
pericalcarine
lateralorbitofrontal
inferiortemporal
fusiform
transversetemporal
middletemporal
inferiorparietal
lingual
cuneus
supramarginal
superiorparietal
superiortemporal
precuneus
parstriangularis
parsorbitalis
precentral
paracentral
isthmuscingulate
postcentral
parsopercularis
posteriorcingulate
caudalanteriorcingulate
temporalpole
entorhinal
parahippocampal
bankssts
insula
frontalpole
rostralanteriorcingulate
lateraloccipital
medialorbitofrontal
superiorfrontal
caudalmiddlefrontal
rostralmiddlefrontal

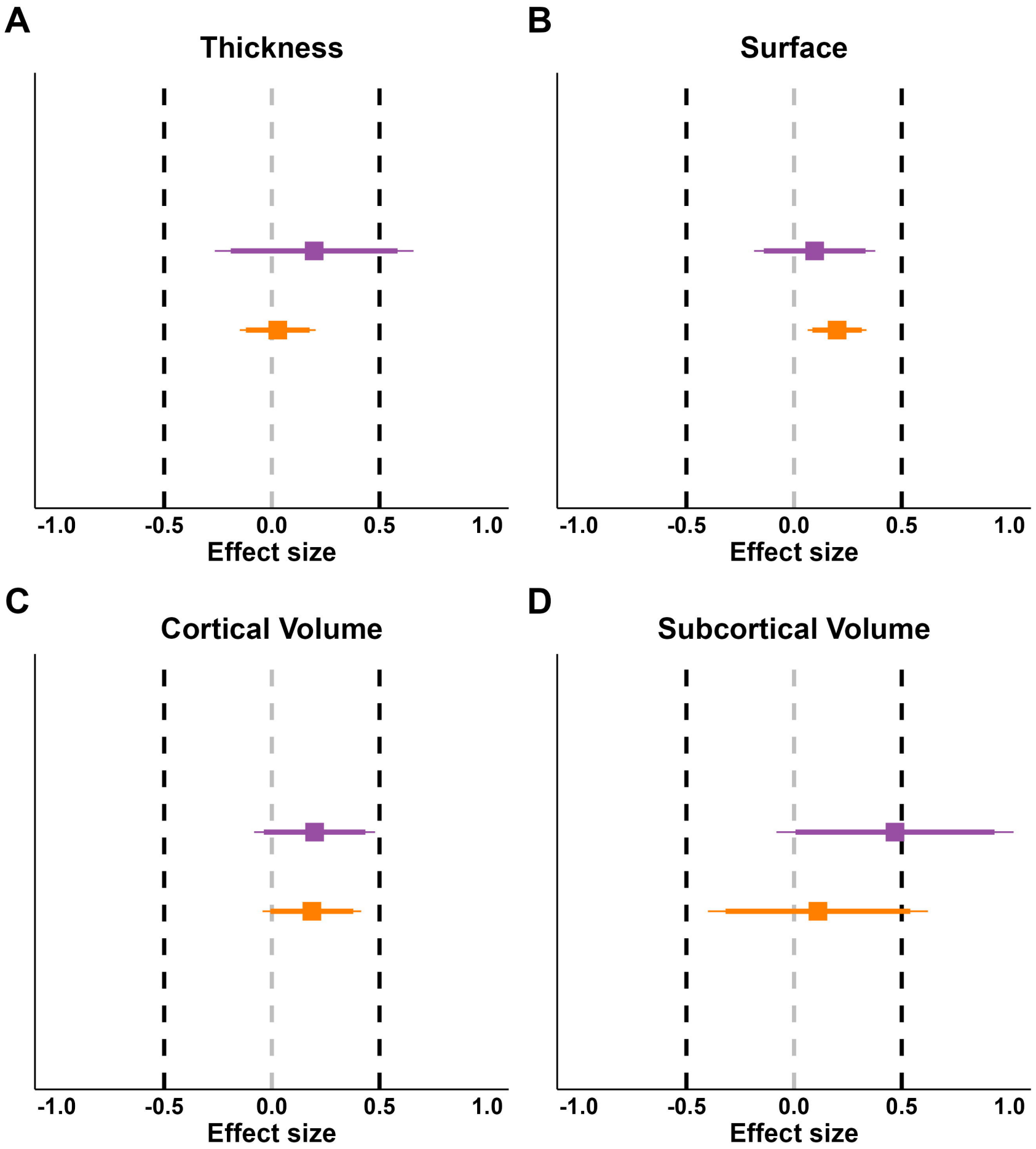
A
Thickness
-1.0
-0.5
0.0
0.5
1.0
Effect size
B
Surface
-1.0
-0.5
0.0
0.5
1.0
Effect size
C
Cortical Volume
-1.0
-0.5
0.0
0.5
1.0
Effect size
D
Subcortical Volume
-1.0
-0.5
0.0
0.5
1.0
Effect size

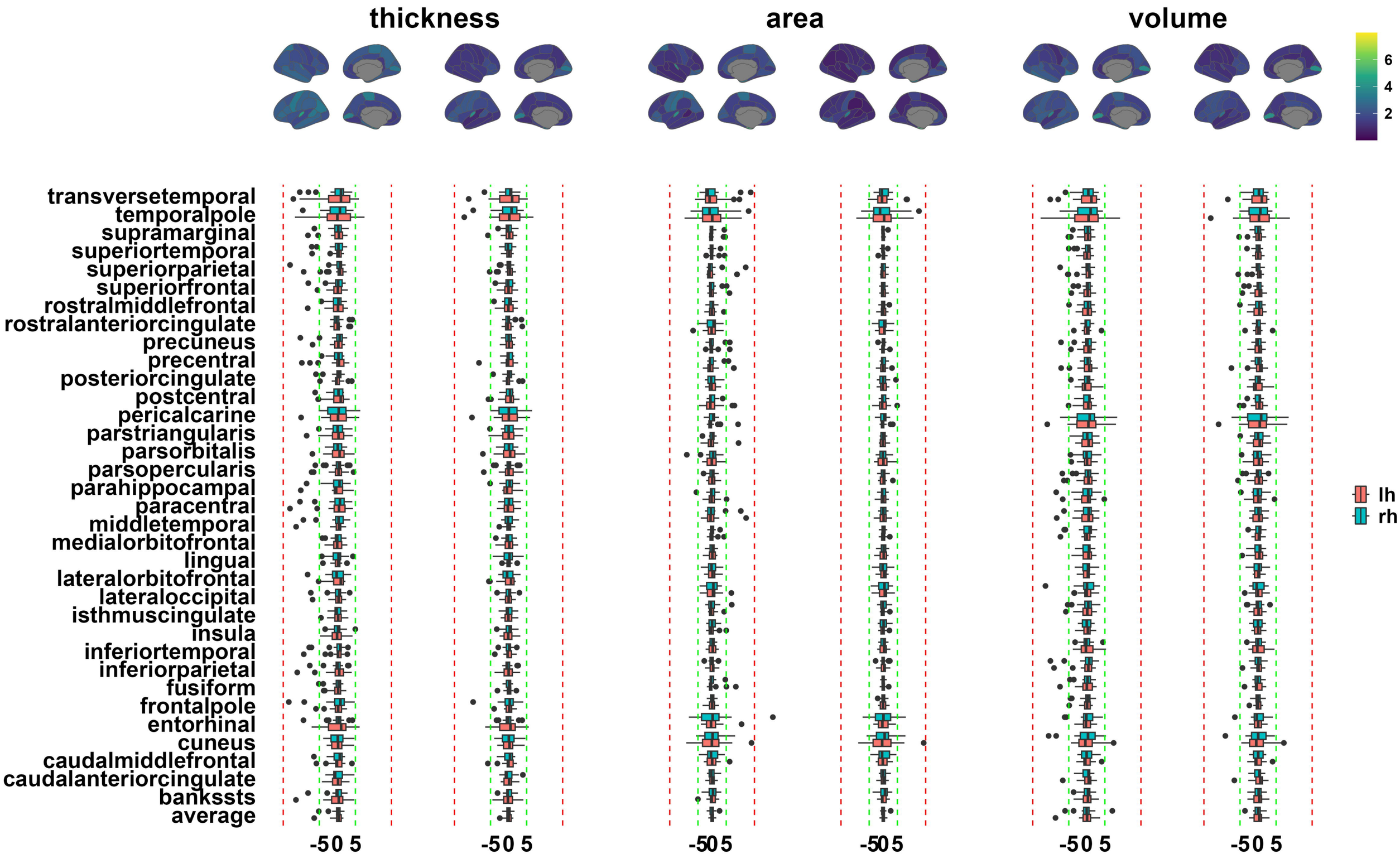
thickness
area
volume
6
4
2
transversetemporal
temporalpole
supramarginal
superiortemporal
superiorparietal
superiorfrontal
rostralmiddlefrontal
rostralanteriorcingulate
precuneus
precentral
posteriorcingulate
postcentral
pericalcarine
parstriangularis
parsorbitalis
parsopercularis
parahippocampal
paracentral
middletemporal
medialorbitofrontal
lingual
lateralorbitofrontal
lateraloccipital
isthmuscingulate
insula
inferiortemporal
inferiorparietal
fusiform
frontalpole
entorhinal
cuneus
caudalmiddlefrontal
caudalanteriorcingulate
bankssts
average
-5 0 5
lh
rh

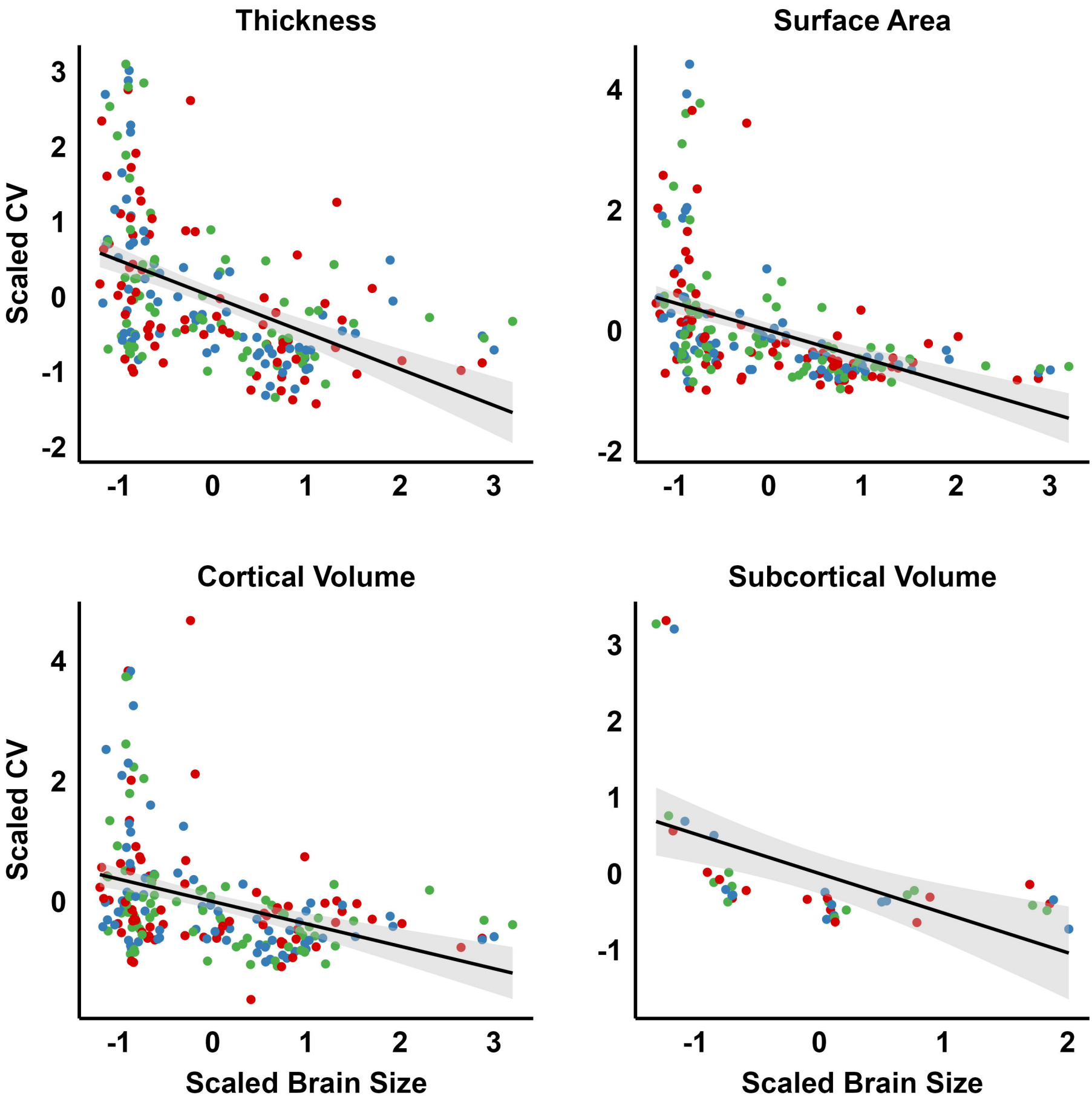
Thickness
Surface Area
Cortical Volume
Subcortical Volume
Scaled CV
Scaled Brain Size
3
2
1
0
-1
-2
4